# Positioning Using Visible Light Communications: A Perspective Arcs Approach

Zhiyu Zhu, Caili Guo, Senior Member, IEEE, Rongzhen Bao, Mingzhe Chen, Member, IEEE, Walid Saad Fellow, IEEE, and Yang Yang, Member, IEEE

#### **Abstract**

Visible light positioning (VLP) is an accurate indoor positioning technology that uses luminaires as transmitters. In particular, circular luminaires are a common source type for VLP, that are typically treated only as point sources for positioning, while ignoring their geometry characteristics. In this paper, the arc feature of the circular luminaire and the coordinate information obtained via visible light communication (VLC) are jointly used for positioning, and a novel perspective arcs approach is proposed for VLC-enabled indoor positioning. The proposed approach does not rely on any inertial measurement unit and has no tilted angle limitation at the user. First, a VLC assisted perspective circle and arc algorithm (V-PCA) is proposed for a scenario in which a complete luminaire and an incomplete one can be captured by the user. Based on plane and solid geometry theory, the relationship between the luminaire and the user is exploited to estimate the orientation and the coordinate of the luminaire in the camera coordinate system. Then, the pose and location of the user in the world coordinate system are obtained by single-view geometry theory. Considering the cases in which parts of VLC links are blocked, an anti-occlusion VLC assisted perspective arcs algorithm (OA-V-PA) is proposed. In OA-V-PA, an approximation method is developed to estimate the projection of the luminaire's center on the image and, then, to calculate the pose and location of the user. Simulation results show that the proposed indoor positioning algorithm can achieve a 90th percentile positioning accuracy of around 10 cm. Moreover, an experimental prototype is implemented to verify the feasibility. In the established prototype, a fused image processing method is proposed to simultaneously obtain the VLC information and the geometric

This research was supported by the U.S. National Science Foundation under Grant CNS-1909372.

- Z. Zhu, R. Bao and Y. Yang are with the Beijing Key Laboratory of Network System Architecture and Convergence, School of Information and Communication Engineering, Beijing University of Posts and Telecommunications, Beijing 100876, China (e-mail: zhuzy@bupt.edu.cn; baorongzhen@bupt.edu.cn; yangyang01@bupt.edu.cn).
- M. Chen is with the Department of Electrical and Computer Engineering and Institute for Data Science and Computing, University of Miami, Coral Gables, FL, 33146, USA (e-mail: mingzhe.chen@miami.edu).
- C. Guo is with Beijing Laboratory of Advanced Information Networks, School of Information and Communication Engineering, Beijing University of Posts and Telecommunications, Beijing 100876, China (e-mail: guocaili@bupt.edu.cn).
- W. Saad is with the Wireless@VT, Bradley Department of Electrical and Computer Engineering, Virginia Tech, Blacksburg, VA, 24060, USA, (email: walids@vt.edu).

A preliminary version of this work [1] appears in the proceeding of IEEE International Conference on Communications (ICC).

information. Experimental results in the established prototype show that the average positioning accuracy is less than 5 cm for different tilted angles of the user.

#### I. Introduction

With the surge of location-based services such as location tracking and navigation, positioning technology has attracted increasing attention from both academia and industry, and it is also drove by the trends of 5G and 6G wireless systems [2]. In the outdoor environment, satellite-based positioning technology can provide acceptable and convenient positioning service. In contrast, existing indoor positioning technologies, such as WiFi, RFID, Ultra-Wide Band (UWB), and Bluetooth still face the challenges of balancing the positioning accuracy and the implementation cost [3]. Since visible light possesses strong directionality and low multipath interference [4], [5], visible light positioning (VLP) with visible light communication (VLC) has emerged as a promising indoor positioning technique with low cost and high positioning accuracy [6].

## A. Related Works

VLP algorithms can be grouped into several categories including: proximity [7], fingerprinting [8]-[10], received signal strength (RSS) [11]–[13], time of arrival (TOA) [14], angle of arrival (AOA) [15], [16] and image sensing [17], [18]. Proximity is the simplest positioning technique. However, it can only provide a proximity location information, whose accuracy largely depends on the density of the transmitter distribution [19]. Both proximity and fingerprinting can estimate the user's location using a single luminaire. The use of fingerprinting can achieve better positioning accuracy than proximity, however, it is susceptible to environment changes [20]. RSS algorithms determine the location of the user based on the power of the received signal, and hence, they depend on accurate channel models [12]. Both TOA and AOA algorithms have high requirements for receiving devices to ensure the positioning accuracy. In particular, TOA needs to use precise clocking unit to ensure accurate time synchronization while AOA needs to use micro-electro-mechanical system sensors to obtain AOA values. Compared to the algorithms that use photodiodes (PD) to receive signals, image sensing algorithms use cameras to receive visible light signals, and they determine the location of a given user by analyzing the geometric relations between LEDs and their projections on the image plane [21], [22]. To this end, an image sensor is used at the receiver to avoid perfect channel model assumption in RSS based algorithms and requirements of receiving devices in TOA and AOA algorithms.

Most existing VLP algorithms achieve positioning by treating indoor luminaires as point sources in indoor scenarios. Hence, they typically need three or more luminaires for positioning [23]–[25]. The

performance of positioning may be limited by the filed of view (FOV) of the user. These approaches neglect the geometric features that the luminaires possess, such as circle and arc features, which can also be used in positioning algorithms and, ultimately, help reduce the number of required luminaires. Recently, the works in [26]–[29] studied circular luminaires based VLP using image sensing. In particular, in [26], the authors assumed a weak perspective projection and marked a margin point on a circular luminaire to estimate the pose and the location of the user. In [27] and [28], the authors proposed positioning models based on inertial measurement unit (IMU) of the camera. [27] proposed a planes-intersection-line positioning scheme by approximating the projected radius of the luminaire, and [28] introduced a center detecting method by using a boundary fitting method. The work in [29] used an IMU and weak perspective projection model to estimate the pose of the user, and the authors showed that this approach improves the accuracy of positioning compared with [26] by calibrating the measurement of IMU so as to reduce the azimuth angle error. Indeed, for the weak perspective projection, a large or small tilted angle can lead to inaccurate approximation, thus resulting in positioning error. The positioning schemes in [27]–[29] relied on an extra device, called IMU, which is known to have inherent measurement errors due to the influence of magnetic field [27]. Overall, existing VLP approaches based on circular luminaires typically require extra devices or assume an ideal projection model, which limits their practical applications. In contrast, we propose a practical indoor positioning algorithm based on circular luminaires, which can achieve high positioning accuracy with a single camera as receiver, and relax the tilted angle limitation at the user.

## B. Contributions

The main contribution of this paper is a new perspective arcs method for VLP that is applied in practical application scenarios. In particular, when a complete circular luminaire and an incomplete one are captured, a perspective circle and arc positioning algorithm assisted by VLC (V-PCA) is proposed, which is preliminarily introduced in our conference version [1]. Meanwhile, when two incomplete circular luminaires are captured, an anti-occlusion perspective arcs algorithm assisted by VLC (OA-V-PA) is proposed for indoor positioning. Compared to our previous work [1], here, we propose a new positioning algorithm, OA-V-PA, to tackle the challenge of occlusion. In addition, we have developed a prototype in order to verify the performance of the algorithm. To authors' best knowledge, this is the first VLP method for circular luminaires that can achieve accurate and practical positioning without IMU and strict tilted angle limitations at the user. Our key contributions are summarized as follows:

• We propose an indoor positioning system with a circular luminaires layout. In the system, a perspective circle and arc algorithm, dubbed V-PCA, is proposed, and the user equipped with a single camera can

be located. In V-PCA, the geometric features consisting of a complete circle and an arc are exploited to obtain the normal vector of the luminaire first. Then, we obtain the projections of the center and a mark point of circular luminaire on the image plane based on solid geometry theory. We finally estimate the location and pose of the user based on single-view geometry theory by analyzing the normal vector and the geometric information of the center and the mark point.

- To further enhance the practicality of V-PCA, we propose an anti-occlusion VLC assisted perspective arcs algorithm (OA-V-PA), which can achieve efficient positioning even when some of the VLC links are blocked. In OA-V-PA, only two arcs extracted from two incomplete luminaires are required to estimate the location and pose of the user. We also show that the positioning system has no requirement of IMU at the user, and it significantly relaxes the tilted angle limitations of the user.
- We implement both simulations and practical experiments to verify the performance of V-PCA and OA-V-PA. In the practical experiments, we use a mobile phone as the receiver, and we propose a fused image processing scheme to receive the visible light signals and detect the contour of the luminaire's projection accurately. Finally, we establish an experimental prototype which can achieve accurate and real-time positioning.

Simulation results show that the proposed algorithms can achieve a 95th percentile location accuracy of less than 10 cm, and experimental results show that the proposed algorithm can achieve an average accuracy within 5 cm.

The rest of the paper is organized as follows. Section II introduces the system model. The proposed V-PCA algorithm is presented in Section III, and the proposed OA-V-PA algorithm is detailed in Section IV. Section V introduces the implementation of the algorithm. Then, simulation and experimental results are presented and discussed in Section VI. Finally, conclusions are drawn in Section VII.

Hereinafter, we adopt the following notations: both matrices and coordinates of points are denoted by capital boldface such as  $\mathbf{R}_{c}^{w}$  and  $\mathbf{P}_{i}^{w}$ , and they can be inferred easily by context. Vectors are denoted by  $\overrightarrow{(\cdot)}$  such as  $\overrightarrow{GM}$ , or small boldface such as  $\mathbf{n}_{LED}^{c}$ . In addition, we use  $(\cdot)'$  to denote projection on the image plane. For instance,  $G'_{e}$  is the projection of  $G_{e}$ . Lines are defined and denoted by two points, such as MN. In addition, the definitions of key system parameters are listed in Table I.

### II. SYSTEM MODEL AND PROBLEM FORMULATION

## A. System Model

We consider an indoor VLP system that consists of a circular panel luminaires layout and one user equipped with a camera, as shown in Fig. 1(a). The circular panel luminaires are mounted on the ceiling

TABLE I SUMMARY OF NOTATIONS

Symbol	Meaning	Symbol	Meaning
$(u_o, v_o)^{\mathrm{T}}$	Pixel coordinate of O <sup>i</sup>	$d_x, d_y$	Physical size of each pixel
f	Focal length	Q	Elliptic parameter matrix
$oldsymbol{P}_i^{ ext{w}}/oldsymbol{P}_i^{ ext{c}}/oldsymbol{P}_i^{ ext{a}}$	Coordinate of point <i>i</i> in WCS/CCS/ACS	$\Pi_e/\Pi_f$	Fitted ellipse of luminaire's projection
M	Mark point of the luminaire	$G_e/G_f$	Center of the circular luminaire
M'	Projection of $M$ on image plane	$G'_e/G'_f$	Projection of $G_e/G_f$ on image plane
Γ	Elliptical cone whose vertex is the	$\Gamma_c$	Conical surface that is the lateral face of
	camera and base is the fitted ellipse		elliptical cone $\Gamma$
$\varphi$ , $\theta$ , $\psi$	Euler angles around $x^{c}$ -axis, $y^{c}$ -axis,	$m{n}_{ ext{LED}}^{ ext{w}}$ /	Normal vector of the luminaire in
	$z^{\mathrm{c}}$ -axis	$m{n}_{ ext{LED}}^{ ext{c}}$ / $m{n}_{ ext{LED}}^{ ext{a}}$	WCS/CCS/ACS
$oldsymbol{R}_{ ext{c}}^{ ext{w}}/oldsymbol{t}_{ ext{c}}^{ ext{w}}$	Pose/location of the camera in WCS	$oldsymbol{R}_{ m c}^{ m a}$	Pose of the camera in ACS (Rotation
	(Rotation matrix/translation vector from		matrix from CCS to ACS)
	CCS to WCS)		

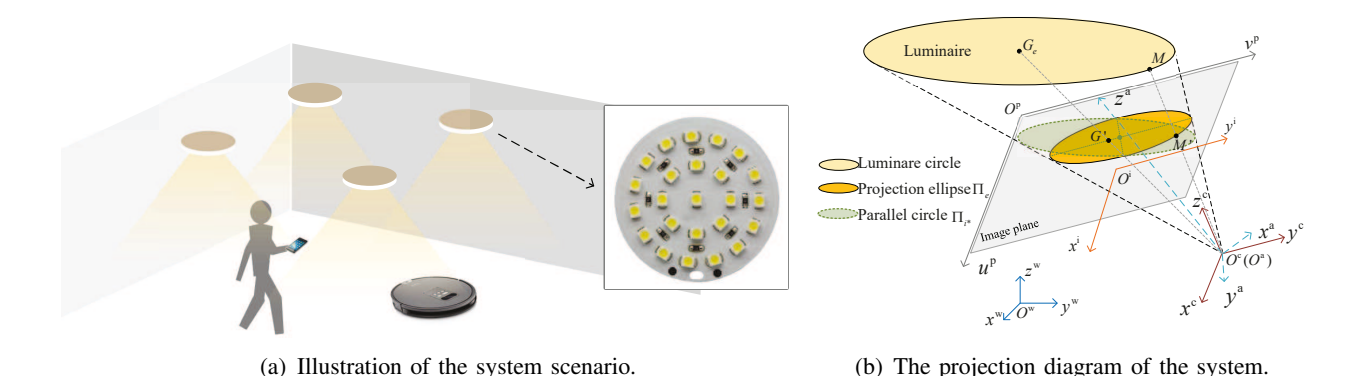


Fig. 1. System model diagrams.

of a room and are assumed to face vertically downwards. Each luminaire consists of several LEDs, each of which transmits the VLC information to the user. The user uses its camera to receive the VLC information and capture the image of the luminaires to estimate its current pose and location.

In the considered system, the geometric relationship between the luminaire and the user will be used to estimate the pose and location of the user. We use a standard pinhole camera model to model the imaging of luminaires [30], [31]. In particular, each luminaire can be captured by the user's camera, and its projection is an ellipse on the image plane as shown in Fig. 1(b). The ellipse  $\Pi_e$  on the image plane is the projection of a luminaire. The projection of the luminaire and the user can generate an elliptical cone  $\Gamma$ , whose base is ellipse  $\Pi_e$ , and vertex is  $O^c$ . The lateral surface of the elliptical cone  $\Gamma$  is a conical surface that is denoted by  $\Gamma_c$ .

To accurately estimate the user's location and pose, we need to use four coordinate systems: a) the two-dimensional (2D) pixel coordinate system (PCS)  $O^p - u^p v^p$  on the image plane, b) the 2D image

coordinate system (ICS)  $O^i - x^i y^i$  on the image plane, c) the three-dimensional (3D) camera coordinate system (CCS)  $O^c - x^c y^c z^c$ , and d) the 3D world coordinate system (WCS)  $O^w - x^w y^w z^w$ . In particular,  $O^p$ ,  $O^i$ ,  $O^c$  and  $O^w$  are the origins of PCS, ICS, CCS and WCS, respectively. In PCS, ICS, and CCS, the coordinate axes  $u^p$ ,  $x^i$ , and  $x^c$  are parallel. Meanwhile,  $v^p$ ,  $y^i$ , and  $y^c$  are parallel. Although PCS and CCS are both on the image plane, their origins  $O^p$  and  $O^i$  are different. In particular,  $O^p$  is at the vertex of the image, while  $O^i$  is at the intersection of the optical axis and the image plane. Meanwhile, the units in ICS, CCS, and WCS are physical units, while the unit of a point in PCS is pixel.  $O^i$  and  $O^c$  are on the optical axis, and the distance between them is the focal length f. Therefore, the z-coordinate of the image plane in CCS is  $z^c = f$ . Here, we term the coordinate of a point in PCS/ICS/CCS/WCS as pixel coordinate/image coordinate/camera coordinate/world coordinate. he positioning process starts with the pixel coordinate since the user first obtains the position of the projection's pixel on the image. Then, the pixel coordinate can be transformed into an image coordinate. Next, we summarize the transformations among the four coordinate systems in the following lemmas.

**Lemma 1.** On the image plane, given a pixel coordinate,  $P_{i'}^{\rm p} = (u_{i'}^{\rm p}, v_{i'}^{\rm p})^{\rm T}$ , of point i' in PCS, the image coordinate,  $P_{i'}^{\rm i} = (x_{i'}^{\rm i}, y_{i'}^{\rm i})^{\rm T}$ , of point i' in ICS can be obtained by

$$\boldsymbol{P}_{i'}^{i} = \begin{bmatrix} x_{i'}^{i} \\ y_{i'}^{i} \end{bmatrix} = \begin{bmatrix} d_{x} & 0 \\ 0 & d_{y} \end{bmatrix} \cdot \boldsymbol{P}_{i'}^{p} - \begin{bmatrix} u_{0}d_{x} \\ v_{0}d_{y} \end{bmatrix}, \tag{1}$$

where  $d_x$  and  $d_y$  are the physical size of each pixel along  $x^i$  and  $y^i$  axes on the image plane, respectively, and  $(u_o, v_o)^T$  is the pixel coordinate of the origin,  $O^i$ , of ICS.

*Proof.* Given the pixel coordinate of the origin,  $(u_o, v_o)^T$ , the physical size,  $d_x$  and  $d_y^1$ , and the pixel coordinate,  $\mathbf{P}_{i'}^{\mathrm{p}} = (u_{i'}^{\mathrm{p}}, v_{i'}^{\mathrm{p}})^T$ , of point i' on the image plane,  $x_{i'}^{\mathrm{i}} = d_x (u_{i'}^{\mathrm{p}} - u_o)$  and  $y_{i'}^{\mathrm{i}} = d_y (v_{i'}^{\mathrm{p}} - v_o)$  can be obtained according to single-view geometry theory [32]. This completes the proof.

**Lemma 2.** Given a camera coordinate,  $P_i^c = (x_i^c, y_i^c, z_i^c)^T$ , of point i in CCS, the image coordinate,

<sup>&</sup>lt;sup>1</sup>The origin  $(u_o, v_o)^T$  and the physical sizes  $d_x$  and  $d_y$ , are camera's intrinsic parameters, and can be calibrated in advance [11].

 ${m P}_{i'}^{\rm i}=(x_{i'}^{\rm i},y_{i'}^{\rm i})^{
m T},$  of its projection point i' on the image plane can be obtained by

$$\mathbf{P}_{i}^{c} = \begin{bmatrix} x_{i}^{c} \\ y_{i}^{c} \\ z_{i}^{c} \end{bmatrix} = z_{i}^{c} \begin{bmatrix} 1/f & 0 & 0 \\ 0 & 1/f & 0 \\ 0 & 0 & 1 \end{bmatrix} \begin{bmatrix} x_{i'}^{i} \\ y_{i'}^{i} \\ 1 \end{bmatrix} = z_{i}^{c} \begin{bmatrix} 1/f & 0 & 0 \\ 0 & 1/f & 0 \\ 0 & 0 & 1 \end{bmatrix} \begin{bmatrix} \mathbf{P}_{i'}^{i} \\ 1 \end{bmatrix}, \tag{2}$$

Particularly, the camera coordinate of point i' in CCS is  $\mathbf{P}_{i'}^{\text{c}} = (x_{i'}^{\text{i}}, y_{i'}^{\text{i}}, f)^{\text{T}}$ .

*Proof.* According to the triangle similarity in projection diagram, we have  $\frac{x_i^c}{x_{i'}^l} = \frac{z_i^c}{f}$  and  $\frac{y_i^c}{y_{i'}^l} = \frac{z_i^c}{f}$ . Hence, we can obtain the coordinates of  $P_i^c$  using  $P_{i'}^i$ . This completes the proof of (2). The image plane is perpendicular to the optical axis, and thus, any point on the image plane has the z-coordinate of  $z^c = f$ . Then, we can have the camera coordinate of point i' as  $P_{i'}^c = (x_{i'}^i, y_{i'}^i, f)^T$ .

**Lemma 3.** Given a camera coordinate,  $P_i^c = (x_i^c, y_i^c, z_i^c)^T$ , of point i, a rotation matrix  $R_c^w$ , and a translation vector  $t_c^w$ , the world coordinate,  $P_i^w = (x_i^w, y_i^w, z_i^w)^T$  of point i can be obtained by [22]

$$P_i^{\mathbf{w}} = R_{\mathbf{c}}^{\mathbf{w}} \cdot P_i^{\mathbf{c}} + t_{\mathbf{c}}^{\mathbf{w}}, \tag{3}$$

where  $\mathbf{R}_{c}^{w}$  is a  $3 \times 3$  matrix, which also represents the pose of the user.  $\mathbf{t}_{c}^{w}$  is a  $3 \times 1$  vector, which also represents the location of the user.

*Proof.*  $\mathbf{R}_{c}^{w}$  contains the rotations corresponding to  $x^{c}$ ,  $y^{c}$ , and  $z^{c}$  axes in CCS. Thus,  $\mathbf{R}_{c}^{w}$  can be considered as the pose of the user. Since  $\mathbf{P}_{i}^{w} = \mathbf{t}_{c}^{w}$  when  $\mathbf{P}_{i}^{c} = (0,0,0)^{T}$  according to (3),  $\mathbf{t}_{c}^{w}$  can be considered as the location of the user.

After establishing the relationships among the four coordinate systems, we can use the geometric information on the image plane to deduce the relationship between the user and the spatial luminaire, so as to estimate the user's location and pose. This design problem will be formulated next.

## B. Problem Formulation

Given the introduced system model, we now introduce our pose and location estimation problem. Our purpose is to obtain accurate  $R_c^w$  and  $t_c^w$  in (3). Let  $R_X$ ,  $R_Y$ , and  $R_Z$  be the rotation matrices around axis  $x^c$ ,  $y^c$ , and  $z^c$ , respectively. Then, the pose of the user can be expressed as

$$\mathbf{R}_{\mathrm{c}}^{\mathrm{w}} = \mathbf{R}_{X} \mathbf{R}_{Y} \mathbf{R}_{Z},\tag{4}$$

where  $R_X$ ,  $R_Y$ , and  $R_Z$  can be denoted by [22]

$$\mathbf{R}_{X} = \begin{bmatrix} 1 & 0 & 0 \\ 0 & \cos \varphi & -\sin \varphi \\ 0 & \sin \varphi & \cos \varphi \end{bmatrix}, \tag{5}$$

$$\boldsymbol{R}_{Y} = \begin{bmatrix} \cos \theta & 0 & \sin \theta \\ 0 & 1 & 0 \\ -\sin \theta & 0 & \cos \theta \end{bmatrix}, \tag{6}$$

and

$$\boldsymbol{R}_{Z} = \begin{bmatrix} \cos \psi & -\sin \psi & 0 \\ \sin \psi & \cos \psi & 0 \\ 0 & 0 & 1 \end{bmatrix}, \tag{7}$$

with  $\varphi$ ,  $\theta$ , and  $\psi$  being the Euler angles around  $x^c$ -axis,  $y^c$ -axis, and  $z^c$ -axis, respectively. Hence, if we want to estimate the pose  $\mathbf{R}_c^w$  of the user, we need to estimate the Euler angles  $\varphi$ ,  $\theta$ , and  $\psi$ . Given the estimated  $\mathbf{R}_c^w$ , the location  $\mathbf{t}_c^w$  of the user can also be estimated according to (3).

We consider two scenarios. In the *first scenario*, we analyze a case in which a complete circular luminaire and an incomplete one can be captured by the camera. As introduced in Section I, when using circular luminaires for positioning in existing studies, an IMU<sup>2</sup> must be used to estimate the Euler angles, the accuracy of which is significantly affected by the estimation deviation of the IMU. Moreover, when circle features are employed in pose estimation, there lacks point correspondences, and there are usually dual solutions. To circumvent these challenges, the V-PCA algorithm is proposed for accurate positioning. We propose two methods including space-time coding and artificially marking to obtain point correspondences. We also propose to use the geometric features extracted from the ellipse image of a circular luminaire to estimate the Euler angles, and use another captured incomplete luminaire for disambiguating. Then, considering that parts of VLC links may be blocked, we further consider a *second scenario* in which two incomplete luminaires are captured. However, the point correspondences in V-PCA are no longer appropriate for this scenario. Hence, we propose the OA-V-PA algorithm with an approximation method developed to solve point correspondences. In the following sections, we detail the proposed V-PCA and OA-V-PA algorithms.

<sup>&</sup>lt;sup>2</sup>IMU is an electronic device that can measure the orientation of the user, and it usually has measurement errors [27].

## III. V-PCA Positioning Algorithm

In this section, we consider a scenario in which a complete luminaire and an incomplete luminaire are simultaneously captured by the camera, and then, a novel positioning algorithm, called V-PCA, is introduced for the user's pose and location estimation. Compared to existing VLP algorithms that require IMU for Euler angles estimation, the proposed algorithm can achieve higher positioning accuracy with only image sensor, thereby avoiding measurement errors. The proposed V-PCA algorithm consists of three steps: a) Estimate the normal vector  $n_{\rm LED}^{\rm c}$  of the luminaire in CCS. b) Estimate the coordinates of the center  $G_e$  and the mark point M in CCS, i.e.,  $P_{G_e}^c$  and  $P_M^c$ . c) Estimate the pose and the location of the user in WCS based on  $m{n}_{\mathrm{LED}}^{\mathrm{c}}, m{P}_{G_e}^{\mathrm{c}}$  and  $m{P}_{M}^{\mathrm{c}}$  by using single-view geometry theory. Next, we introduce the various steps of our proposed V-PCA algorithm.

## A. Normal Vector of Luminaires in CCS

To estimate the pose and location of the user, the first step is to find the normal vector  $n_{\mathrm{LED}}^{\mathrm{c}}$  of the luminaire in CCS, and, thus, determine the orientation of the user. To obtain  $n_{
m LED}^{
m c}$ , we establish an auxiliary coordinate system (ACS) and exploit the geometric relation between the luminaire and its projection on the image plane.

On the image plane, the elliptic curve  $\Pi_e$  of a luminaire can be expressed as

$$A(x^{i})^{2} + Bx^{i}y^{i} + C(y^{i})^{2} + Dx^{i} + Ey^{i} + 1 = 0,$$
(8)

where A, B, C, D, and E are parameters that can be determined by curving fitting with the least squares fitting [33]. We use the singular value decomposition method to solve this least squares fitting problem, and the computational complexity is  $\mathcal{O}(nm)$  [34], where m is the number of extracted feature points, and n is the number of fitted parameters.

**Lemma 4.** Given ICS, CCS and an expression of elliptic curve,  $\Pi_e$ , i.e.,  $A(x^i)^2 + Bx^iy^i + C(y^i)^2 + Dx^i + Dx^iy^i +$  $Ey^{i} + 1 = 0$ , there must exist a canonical frame of conicoid, i.e., ACS, which enables the conical surface  $\Gamma_c$  of the elliptical cone  $\Gamma$  can be represented in a compact form as

$$\lambda_1(x^{a})^2 + \lambda_2(y^{a})^2 + \lambda_3(z^{a})^2 = 0, (9)$$

in ACS.  $\lambda_1,\lambda_2$ , and  $\lambda_3$  are eigenvalues of  ${\bf Q}=\begin{bmatrix}Af^2&Bf^2/2&Df/2\\Bf^2/2&Cf^2&Ef/2\\Df/2&Ef/2&1\end{bmatrix}$ , and the rotation matrix from ACS to CCS is denoted by  ${\bf R}_{\rm a}^c$ , which consists of the eigenvectors of  ${\bf Q}$ .

*Proof.* By substituting (2) into (8), we can have a general form of the conical surface  $\Gamma_c$  in CCS as

$$Af^{2}(x^{c})^{2} + Bf^{2}x^{c}y^{c} + Cf^{2}(y^{c})^{2} + Dfx^{c}z^{c} + Efy^{c}z^{c} + (z^{c})^{2} = \begin{bmatrix} x^{c} & y^{c} & z^{c} \end{bmatrix} \mathbf{Q} \begin{bmatrix} x^{c} & y^{c} & z^{c} \end{bmatrix}^{T} = 0, \quad (10)$$

where 
$$\mathbf{Q}=\begin{bmatrix}Af^2 & Bf^2/2 & Df/2\\Bf^2/2 & Cf^2 & Ef/2\\Df/2 & Ef/2 & 1\end{bmatrix}$$
. Matrix  $\mathbf{Q}$  is not a diagonal matrix since the central axis of

elliptical cone  $\Gamma$  does not coincide with any coordinate axes of CCS. To simplify (10), we first assume a canonical frame of conicoid, ACS, and a rotation matrix,  $R_a^c$ , from ACS to CCS. Then, the transformation between ACS and CCS can be expressed as

$$\begin{bmatrix} x^{c} & y^{c} & z^{c} \end{bmatrix}^{T} = \mathbf{R}_{a}^{c} \begin{bmatrix} x^{a} & y^{a} & z^{a} \end{bmatrix}^{T}, \tag{11}$$

By substituting (11) into (10), we have

$$\begin{bmatrix} x^{\mathbf{a}} & y^{\mathbf{a}} & z^{\mathbf{a}} \end{bmatrix} (\mathbf{R}_{\mathbf{a}}^{\mathbf{c}})^{\mathrm{T}} \mathbf{Q} \mathbf{R}_{\mathbf{a}}^{\mathbf{c}} \begin{bmatrix} x^{\mathbf{a}} & y^{\mathbf{a}} & z^{\mathbf{a}} \end{bmatrix}^{\mathrm{T}} = 0.$$
 (12)

Next, by diagonalizing matrix  $\mathbf{Q}$ , (12) can be derived as

$$(\mathbf{R}_{a}^{c})^{T} \mathbf{Q} \mathbf{R}_{a}^{c} = (\mathbf{R}_{a}^{c})^{-1} \mathbf{Q} \mathbf{R}_{a}^{c} = \operatorname{diag}(\lambda_{1}, \lambda_{2}, \lambda_{3}),$$
(13)

where  $R_a^c$  consists of the eigenvectors of Q. In addition,  $\lambda_1, \lambda_2$ , and  $\lambda_3$  are eigenvalues of Q. Hence, in ACS, a compact form equation of conical surface  $\Gamma_c$  in (9) can be derived from (12).

Note that matrix Q is a real symmetric matrix, and thus it can be diagonalized definitely. After diagonalizing matrix Q,  $R_a^c$  and  $\lambda_i$ , i=1,2,3 can be obtained. Meanwhile, the corresponding ACS can also be determined.

ACS aligns one of the coordinate axes with the central axis of elliptical cone  $\Gamma$ , and it also shares the same origin with CCS. The values of  $\lambda_i$ , i=1,2,3 determine the relative position of the elliptical cone  $\Gamma$  and the coordinate axes of ACS.  $\Gamma_c$  in (9) is the standard form of a quadric cone in a canonical frame of conicoids [35]. Hence, the coefficients  $\lambda_i$ , i=1,2,3 must contain one negative coefficient and two positive coefficients [36]. Here, six possible cases of  $\lambda_1$ ,  $\lambda_2$ , and  $\lambda_3$  are listed in Table II. Each case represents a relation between the elliptical cone and the coordinate axes. For instance,  $\lambda_3 < 0 < \lambda_2 \le \lambda_1$  means that the central axis of elliptical cone  $\Gamma$  aligns with  $z^a$  axis, the major-axis of the ellipse is parallel to  $y^a$  axis, and the minor-axis is parallel to  $x^a$  axis. When  $\lambda_1$ ,  $\lambda_2$ , and  $\lambda_3$  have other relations, we can always find the corresponding relations between the elliptical cone and the coordinate axes.

TABLE II  $\text{ALL CASES OF } \lambda_i, i=1,2,3.$ 

Cases	Calculation expressions
$\lambda_3 < 0 < \lambda_2 < \lambda_1$	$k_1 = \sqrt{\frac{\lambda_1 - \lambda_2}{\lambda_2 - \lambda_3}}$ , $k_2 = -\sqrt{\frac{\lambda_1 - \lambda_2}{\lambda_2 - \lambda_3}}$
$\lambda_3 < 0 < \lambda_1 < \lambda_2$	$k_1 = \sqrt{\frac{\lambda_2 - \lambda_1}{\lambda_1 - \lambda_3}}$ , $k_2 = -\sqrt{\frac{\lambda_2 - \lambda_1}{\lambda_1 - \lambda_3}}$
$\lambda_2 < 0 < \lambda_1 < \lambda_3$	$k_1 = \sqrt{\frac{\lambda_3 - \lambda_1}{\lambda_1 - \lambda_2}}$ , $k_2 = -\sqrt{\frac{\lambda_3 - \lambda_1}{\lambda_1 - \lambda_2}}$
$\lambda_2 < 0 < \lambda_3 < \lambda_1$	$k_1 = \sqrt{\frac{\lambda_1 - \lambda_3}{\lambda_3 - \lambda_2}}$ , $k_2 = -\sqrt{\frac{\lambda_1 - \lambda_3}{\lambda_3 - \lambda_2}}$
$\lambda_1 < 0 < \lambda_3 < \lambda_2$	$k_1 = \sqrt{\frac{\lambda_2 - \lambda_3}{\lambda_3 - \lambda_1}}$ , $k_2 = -\sqrt{\frac{\lambda_2 - \lambda_3}{\lambda_3 - \lambda_1}}$
$\lambda_1 < 0 < \lambda_2 < \lambda_3$	$k_1 = \sqrt{\frac{\lambda_3 - \lambda_2}{\lambda_2 - \lambda_1}}$ , $k_2 = -\sqrt{\frac{\lambda_3 - \lambda_2}{\lambda_2 - \lambda_1}}$

We estimate the normal vector of the luminaire plane by finding a parallel plane to it. In particular, rotating the plane that ellipse  $\Pi_e$  lies on around its major axis, we can obtain two circles, termed as  $\Pi_1$  and  $\Pi_2$ , that intersect with conical surface  $\Gamma_c$ , and only one of them is parallel to the luminaire.  $\Pi_1$  and  $\Pi_2$  have different orientations, and both circles are parallel to  $y^a$  axis. Without loss of generality, we define planes  $\Pi_1$  and  $\Pi_2$  as

$$z^{\mathbf{a}} = k_1 x^{\mathbf{a}} + b, \tag{14}$$

and

$$z^{\mathbf{a}} = k_2 x^{\mathbf{a}} + b, \tag{15}$$

respectively, where  $k_1 = \sqrt{\frac{\lambda_1 - \lambda_2}{\lambda_2 - \lambda_3}}$  and  $k_2 = -\sqrt{\frac{\lambda_1 - \lambda_2}{\lambda_2 - \lambda_3}}$  decide the orientation of the circular planes [35], and b is a constant. The expressions of  $k_1$  and  $k_2$  for all cases are listed in Table II. Given variables  $k_1$  and  $k_2$ , there exists two possible normal vectors of the luminaire, and they can be expressed as  $\boldsymbol{n}_{\Pi_1}^a = (k_1, 0, -1)^T$  and  $\boldsymbol{n}_{\Pi_2}^a = (k_2, 0, -1)^T$ .

To eliminate the duality of the normal vector, an arc of another LED luminaire is utilized to find the correct one, instead of requiring another complete luminaire. This arc can be fitted into another ellipse  $\Pi_f$ . Similarly, we further construct the elliptical cone using  $\Pi_f$  and the camera vertex, and rotate the plane that  $\Pi_f$  lies on to obtain two circles with the normal vectors of  $\boldsymbol{n}_{\Pi_3}^{\rm a}$  and  $\boldsymbol{n}_{\Pi_4}^{\rm a}$ . Since both the arc and the complete circle are on the ceiling of the room, there exists two identical items among  $\boldsymbol{n}_{\Pi_1}^{\rm a}$ ,  $\boldsymbol{n}_{\Pi_2}^{\rm a}$ ,  $\boldsymbol{n}_{\Pi_3}^{\rm a}$ , and  $\boldsymbol{n}_{\Pi_4}^{\rm a}$  in theory. Then, we can solve

$$\min_{i,j} \left\| \boldsymbol{n}_{\Pi_i}^{\mathbf{a}} - \boldsymbol{n}_{\Pi_j}^{\mathbf{a}} \right\|, i = 1, 2, j = 3, 4, \tag{16}$$

to obtain the optimal plane  $\Pi_{i^*}$  and the normal vector  $\boldsymbol{n}_{\Pi_{i^*}}^{\mathrm{a}}$ , where  $i^*$  represents the optimal i obtained

from (16). Based on  $n_{\Pi_{i^*}}^a$ , the normalized normal vector of the LED luminaire in CCS can be expressed as

$$n_{\text{LED}}^{\text{c}} = R_{\text{a}}^{\text{c}} \frac{n_{\Pi_{i^*}}^{\text{a}}}{\sqrt{k_{i^*}^2 + 1}}.$$
 (17)

As such, the normal vector of the luminaires can be obtained, and it will be used in the subsequent pose and location estimation. For convenience, we denote the obtained  $\mathbf{n}_{\text{LED}}^{\text{c}}$  in (17) as  $\mathbf{n}_{\text{LED}}^{\text{c}} = (t_1, t_2, t_3)^{\text{T}}$ .

## B. Center and Mark Point Coordinates in CCS

To achieve positioning, two points,  $G_e$  and M, on the luminaire are required, and their coordinates in CCS,  $\mathbf{P}_{G_e}^c$  and  $\mathbf{P}_{M}^c$ , should be obtained. In particular,  $G_e$  is at the center of the luminaire, while M is a mark point on the margin of the luminaire. The vector  $\overrightarrow{G_eM}$  can be normalized as  $\mathbf{n}_{G_eM}^w = (0,1,0)^T$  in WCS. In this section, we leverage the geometric relationship between the points and their projections on the image plane to estimate  $\mathbf{P}_{G_e}^c$  and  $\mathbf{P}_{M}^c$ .

We first propose to obtain the projections of  $G_e$  and M on the image plane.  $G'_e$  and M' are the projections of  $G_e$  and M, respectively. There are two methods to obtain the projections proposed. The first method is to artificially mark. The points can be marked directly on the luminaire, as implemented in [26]. The second method designs a space-time coding model to obtain points  $G'_e$  and M' by taking advantage of VLC. One possible space-time coding model is designed as shown in Fig. 2. The codes are sequentially transmitted by the luminaire. It can be found that the projection point  $G'_e$  is the intersection point of lines  $P'G'_e$  and  $M'G'_e$ . Lines  $P'G'_e$  and  $M'G'_e$  are the projections of lines  $PG_e$  and  $MG_e$ , respectively. The projection point M' can be found as the endpoint of the overlapped line,  $M'G'_e$ , of two sequential codes. Thus, the points  $G'_e$  and M' can be found on the image plane, and their coordinates can be obtained through image processing [37]. Even though in Fig. 2 there are only a few active LEDs, the space-time coding design will not affect the illumination level. This is because that the space-time coding can be carefully designed to achieve a target dimming level [38]. In addition, all the LEDs on the same luminaire broadcast the luminaire's ID information and the world coordinates information of the center  $G_e$  and the mark point M. In addition to the above method, one can use other space-time codes such as turning on/off the center LED and the mark point to identify the mark points.

Then, we exploit the relationship between the points and their projections to obtain  $P_{G_e}^c$  and  $P_M^c$ . As shown in Fig. 1(b), the luminaire plane intersects line  $M'O^c$  at point M, while intersects line  $G'_eO^c$  at point  $G_e$ . Hence, we now derive equations of the luminaire plane and the lines.

Fig. 3 shows the projection of elliptical cone  $\Gamma$  on the  $x^aOz^a$  plane. Line segment  $L_1L_2$  is the projection of the complete luminaire circle captured by the camera, and the length of  $L_1L_2$  is equal to the diameter

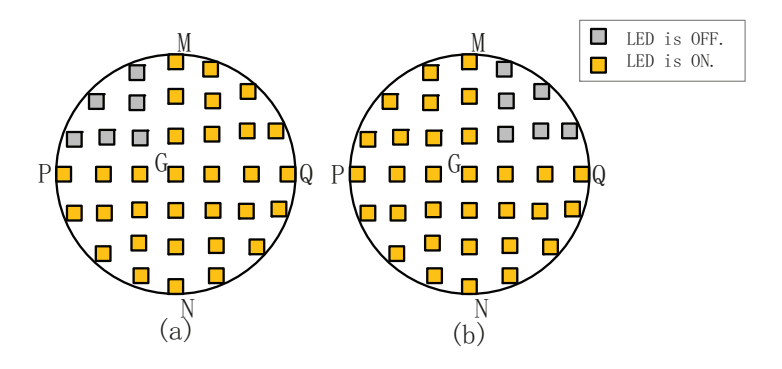


Fig. 2. Space-time coding model.

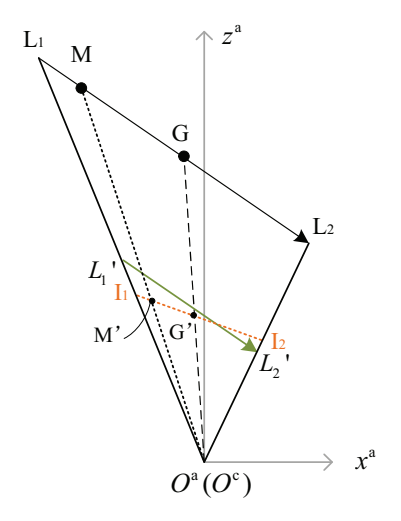


Fig. 3. The projection of elliptical cone on the  $x^{a}Oz^{a}$  plane.

of the luminaire, 2R. Line segment  $I_1I_2$  is the projection of  $\Pi_e$  on  $x^aOz^a$  plane, and line segment  $L_1'L_2'$ is the projection of  $\Pi_{i^*}$  on  $x^{\rm a}Oz^{\rm a}$  plane. Moreover, lines  $L_1O^{\rm a}$  and  $L_2O^{\rm a}$  can be expressed as [35]

$$z^{\mathbf{a}} = \pm \sqrt{-\frac{\lambda_1}{\lambda_3}} x^{\mathbf{a}}.$$
 (18)

By combining and solving  $z^{\mathbf{a}}=k_{i^*}x^{\mathbf{a}}+b$  and (18), the coordinates of points  $L_1'$  and  $L_2'$  can be obtained. Here, we define  $\boldsymbol{P}_{L_1'}^{\mathbf{a}}=\left(x_{L_1'}^{\mathbf{a}},y_{L_1'}^{\mathbf{a}},z_{L_1'}^{\mathbf{a}}\right)^{\mathrm{T}}$  and  $\boldsymbol{P}_{L_2'}^{\mathbf{a}}=\left(x_{L_2'}^{\mathbf{a}},y_{L_2'}^{\mathbf{a}},z_{L_2'}^{\mathbf{a}}\right)^{\mathrm{T}}$ . The expression of luminaire plane can be given by

$$z^{\mathbf{a}} = k_{\text{LED}} x^{\mathbf{a}} + b_{\text{LED}},\tag{19}$$

where  $k_{\text{LED}} = k_{i^*}$  and  $b_{\text{LED}} = \frac{2R \cdot b}{\left\| \mathbf{P}_{L_1'}^{\text{a}} - \mathbf{P}_{L_2'}^{\text{a}} \right\|}$ .

The coordinate,  $\mathbf{P}_{M'}^{\text{c}}$ , of point M' in CCS can be obtained by (2). Then, the coordinate,  $\mathbf{P}_{M'}^{\text{a}} = \mathbf{P}_{M'}^{\text{a}}$ 

 $(x_{M'}^{\rm a},y_{M'}^{\rm a},z_{M'}^{\rm a})^{\rm T}$ , of point M' in ACS can be further obtained by  $P_{M'}^{\rm a}=R_{\rm c}^{\rm a}\cdot P_{M'}^{\rm c}$ . With  $P_{M'}^{\rm a}=(x_{M'}^{\rm a},y_{M'}^{\rm a},z_{M'}^{\rm a})^{\rm T}$ , the point-normal form equation of line  $M'O^{\rm a}$  can be given by

$$\frac{x^{\mathbf{a}}}{x_{M'}^{\mathbf{a}}} = \frac{y^{\mathbf{a}}}{y_{M'}^{\mathbf{a}}} = \frac{z^{\mathbf{a}}}{z_{M'}^{\mathbf{a}}}.$$
 (20)

From Fig. 3, we can also observe that luminaire plane and line  $M'O^a$  intersect at point M. Thus by combining and solving (19) and (20), we can obtain the coordinate of point M in ACS, i.e.,  $\mathbf{P}_{M}^{a}$ . Similarly, we can also obtain the coordinate of point  $G_e$ ,  $\mathbf{P}_{G_e}^{a}$ , in ACS by using the line  $G'O^a$  and (19). Finally, the coordinates of points  $G_e$  and M in CCS,  $\mathbf{P}_{G_e}^{c}$  and  $\mathbf{P}_{M}^{c}$ , are given by  $\mathbf{P}_{G_e}^{c} = \mathbf{R}_{a}^{c} \cdot \mathbf{P}_{G_e}^{a}$  and  $\mathbf{P}_{M}^{c} = \mathbf{R}_{a}^{c} \cdot \mathbf{P}_{M}^{a}$ , respectively.

## C. Pose and Location Estimation

Based on  $n_{\text{LED}}^{\text{c}}$ ,  $P_{G_e}^{\text{c}}$  and  $P_M^{\text{c}}$ , the pose and location of the user in WCS can be further obtained with VLC as follows.

Based on single-view geometry theory, the relationship between  $\boldsymbol{n}_{\text{LED}}^{\text{c}} = (t_1, t_2, t_3)^{\text{T}}$  and  $\boldsymbol{n}_{\text{LED}}^{\text{w}} = (0, 0, -1)^{\text{T}}$  is  $\boldsymbol{n}_{\text{LED}}^{\text{c}} = (\boldsymbol{R}_{\text{c}}^{\text{w}})^{\text{T}} \cdot \boldsymbol{n}_{\text{LED}}^{\text{w}}$ , which can further derived as

$$\begin{cases}
\sin \theta = t_1, \\
-\cos \theta \sin \varphi = t_2, \\
-\cos \theta \cos \varphi = t_3.
\end{cases}$$
(21)

The rotation angles  $\varphi$  and  $\theta$  corresponding to the  $x^c$ -axis and  $y^c$ -axis can be obtained by solving (21). In addition,  $\overrightarrow{G_eM}$  can be normalized as  $\boldsymbol{n}_{G_eM}^{\mathrm{w}} = (0,1,0)^{\mathrm{T}}$  in WCS. The normalized form of  $\overrightarrow{G_eM}$  will be  $\boldsymbol{n}_{G_eM}^{\mathrm{c}} = \frac{\boldsymbol{P}_{G_e}^{\mathrm{c}} - \boldsymbol{P}_{M}^{\mathrm{c}}}{\|\boldsymbol{P}_{G_e}^{\mathrm{c}} - \boldsymbol{P}_{M}^{\mathrm{c}}\|} = (s_1, s_2, s_3)^{\mathrm{T}}$ . We also have  $\boldsymbol{n}_{G_eM}^{\mathrm{w}} = \boldsymbol{R}_{\mathrm{c}}^{\mathrm{w}} \cdot \boldsymbol{n}_{G_eM}^{\mathrm{c}}$ , which can be further derived as

$$\begin{cases} \sin \psi \cos \theta = s_1, \\ \cos \psi \cos \varphi + \sin \psi \sin \theta \sin \varphi = s_2, \\ -\cos \psi \sin \varphi + \sin \psi \sin \theta \cos \varphi = s_3. \end{cases}$$
 (22)

Then, with the obtained  $\varphi$  and  $\theta$ , the rotation angle  $\psi$  corresponding to  $z^c$ -axis can be obtained from (22). Note that all the three equations are needed to determine a unique angle.  $\mathbf{R}_c^w$  can also be obtained according to (4). By substituting the obtained WCS and CCS coordinates of G and M, i.e.,  $\mathbf{P}_{G_e}^w$ ,  $\mathbf{P}_{G_e}^c$ ,  $\mathbf{P}_{M}^w$  and  $\mathbf{P}_{M}^c$ , into

$$\boldsymbol{t}_{c}^{w} = \frac{1}{2} \left[ \left( \boldsymbol{P}_{G_{e}}^{w} - \boldsymbol{R}_{c}^{w} \cdot \boldsymbol{P}_{G_{e}}^{c} \right) + \left( \boldsymbol{P}_{M}^{w} - \boldsymbol{R}_{c}^{w} \cdot \boldsymbol{P}_{M}^{c} \right) \right], \tag{23}$$

 $\mathbf{t}_{c}^{w}$  can be obtained. In (23), we average  $\mathbf{t}_{c}^{w} = \mathbf{P}_{G_{e}}^{w} - \mathbf{R}_{c}^{w} \cdot \mathbf{P}_{G_{e}}^{c}$  and  $\mathbf{t}_{c}^{w} = \mathbf{P}_{M}^{w} - \mathbf{R}_{c}^{w} \cdot \mathbf{P}_{M}^{c}$  to reduce estimation errors. In this way, the pose and location of the camera, i.e.,  $\mathbf{R}_{c}^{w}$  and  $\mathbf{t}_{c}^{w}$ , have been obtained.

### IV. AO-V-PA POSITIONING ALGORITHM

In Section III, an accurate positioning algorithm V-PCA has been proposed. However, in practice, the camera may not always be able to capture complete circular luminaire images due to limited FOV and possible occlusions. In such circumstances, the center of luminaire and the mark point cannot be determined by the space-time coding design or artificial marking, and, thus, V-PCA cannot work. To circumvent these practical challenges, we propose an anti-occlusion positioning algorithm based on V-PCA, called AO-V-PA, which can achieve positioning using incomplete circular luminaire images. In particular, the normal vector of the luminaire in CCS is first estimated using the same process as V-PCA. Then, we fit the ellipses from arcs, and the center of the ellipse is approximated as the projection of the luminaires's center on the image plane. Finally, the pose and location of the user can be obtained based on the estimated centers and the normal vector  $n_{\text{LED}}^{\text{c}}$ . Since the principle of  $n_{\text{LED}}^{\text{c}}$  estimation in OA-V-PA is similar to the one in V-PCA, we will not reproduce it in this section for brevity. The main differences between OA-V-PA and V-PCA are introduced below.

### A. Center Coordinates in CCS

The image plane has only incomplete luminaires that are defined as incomplete ellipses. In such circumstances, the artificial mark point may not be captured, and the space-time coding can also not be completely received. Thus, we propose to approximate the projection of the luminaire's center using the center of the fitted ellipse, so as to calculate the pose of the user. Although the approximation of the projection center may yield additional estimation errors, it can increase the feasibility and robustness of the positioning algorithm, which will be verified in the simulation results.

We use  $G_e$  and  $G_f$  to represent the centers of two circular luminaires, which are captured by the camera and lie on two ellipses,  $\Pi_e$  and  $\Pi_f$ , respectively on the image plane. The projections of  $G_e$  and  $G_f$  on the image plane are  $G'_e$  and  $G'_f$ , respectively. The general form functions of ellipses  $\Pi_e$  and  $\Pi_f$  can be estimated according to (8). Then, the known parameters A, B, C, D, and E can be used to obtain the centers of the ellipses. The coordinate of the center of ellipse  $\Pi_e$  in ICS can be expressed as

$$\begin{cases} x_e^{i} = \frac{BE - 2CD}{4AC - B^2}, \\ y_e^{i} = \frac{BD - 2AE}{4AC - B^2}, \end{cases}$$
 (24)

and it can be used to approximate  $P_{G'_e}^i \approx \left(x_e^i, y_e^i\right)^T$ . Similarly, the center of another fitted ellipse  $\Pi_f$  on the image plane can also be approximated with  $P_{G'_f}^i \approx \left(x_f^i, y_f^i\right)^T$ . Next,  $P_{G'_e}^i$  and  $P_{G'_f}^i$  are respectively used to obtain the point-normal form equations of lines  $G'_eO^a$  and  $G'_fO^a$ , which are combined and solved with (19) to obtain the coordinates of the point  $G_e$  and  $G_f$  in ACS. Thus, we obtain the coordinates,  $P_{G_e}^a$  and  $P_{G_f}^a$ , which are respectively substituted into  $P_{G_e}^c = R_a^c \cdot P_{G_e}^a$  and  $P_{G_f}^c = R_a^c \cdot P_{G_f}^a$  to obtain  $P_{G_e}^c$  and  $P_{G_f}^c$ . Consequently, the coordinates of two luminaires' centers in CCS can be estimated.

## B. Pose and Location Estimation

This step estimates the pose and location of the user. Similar to Section III, we first calculate the rotation matrix. The rotation angles  $\varphi$  and  $\theta$  corresponding to the  $x^c$ -axis and  $y^c$ -axis can be obtained according to (21). The rotation angle  $\psi$  corresponding to the  $z^c$ -axis can be obtained by using the estimated luminaires' centers, i.e.,  $G_e$  and  $G_f$ . In particular, the normalized form of  $\overline{G_eG_f}$  in WCS is calculated first with the known  $P_{G_e}^{\rm w}$  and  $P_{G_f}^{\rm w}$ , and we denote it by  $n_{G_eG_f}^{\rm w} = (g_1, g_2, g_3)^{\rm T}$  for simplicity. Note that  $(g_1, g_2, g_3)^{\rm T}$  cannot be equal to  $(0, 1, 0)^{\rm T}$ . This is because that  $\overline{G_eG_f}$  can have arbitrary direction since the camera may capture two luminaires at any locations. Then, the normalized form of  $\overline{G_eG_f}$  in CCS is calculated by  $n_{G_eG_f}^{\rm c} = \frac{P_{G_e}^{\rm c} - P_{G_f}^{\rm c}}{\|P_{G_e}^{\rm c} - P_{G_f}^{\rm c}\|} = (h_1, h_2, h_3)^{\rm T}$ . According to  $n_{G_eG_f}^{\rm c} = (R_c^{\rm w})^{\rm T} \cdot n_{G_eG_f}^{\rm w}$ , we have

$$\begin{cases} g_1 \cos \psi \cos \theta + g_2 \sin \psi \cos \theta - g_3 \sin \theta = h_1, \\ -g_1 \left( \sin \psi \cos \varphi + \cos \psi \sin \theta \sin \psi \right) + g_2 \left( \cos \psi \cos \varphi + \sin \psi \sin \theta \sin \psi \right) + g_3 \cos \theta \sin \varphi = h_2, \\ g_1 \left( \sin \psi \sin \varphi + \sin \psi \sin \theta \cos \varphi \right) - g_2 \left( \cos \psi \sin \varphi + \sin \psi \sin \theta \cos \varphi \right) + g_3 \cos \theta \cos \varphi = h_3. \end{cases}$$
 (25)

Then, with the obtained  $\varphi$  and  $\theta$ , the rotation angle  $\psi$  corresponding to  $z^c$ -axis can be calculated by using the auxiliary angle formula in trigonometric function to solve (25).  $\mathbf{R}_{c}^{w}$  can also be obtained according to (4).

Similar to (23),  $t_c^w$  can be calculated by substituting the obtained WCS and CCS coordinates of  $G_e$  and  $G_f$ , i.e.,  $P_{G_e}^w$ ,  $P_{G_e}^c$ ,  $P_{G_f}^w$ , and  $P_{G_f}^c$ , into

$$\boldsymbol{t_{c}^{w}} = \frac{1}{2} \left[ \left( \boldsymbol{P}_{G_{e}}^{w} - \boldsymbol{R}_{c}^{w} \cdot \boldsymbol{P}_{G_{e}}^{c} \right) + \left( \boldsymbol{P}_{G_{f}}^{w} - \boldsymbol{R}_{c}^{w} \cdot \boldsymbol{P}_{G_{f}}^{c} \right) \right]. \tag{26}$$

Consequently, the pose and location of the user, i.e.,  $R_{\rm c}^{\rm w}$  and  $t_{\rm c}^{\rm w}$ , have been estimated.

Above all, we can observe that V-PCA and OA-V-PA share most of the positioning process, while have some key differences. In particular, when a complete circular luminaire and an incomplete circular luminaire are captured by the camera, the V-PCA can be used to estimate the location; if there are only incomplete circular luminaires captured, the OA-V-PA can be used. Although both V-PCA and OA-V-PA

can be implemented in the same scenarios, OA-V-PA cannot replace V-PCA since V-PCA can directly use the information of the projections of the center and the mark point, while in OA-V-PA, the projection of the luminaire's center is obtained by an approximation method. Hence, V-PCA can provide more accurate positioning results compared to OA-V-PA. The performance difference will be shown in Section VI. Here, we term this dynamic integration of V-PCA and OA-V-PA as V-PA, which can select appropriate positioning algorithms according to the captured luminaires.

### V. IMPLEMENTATION OF V-PA

In this section, we establish an experimental prototype to verify the feasibility and efficiency of the proposed algorithm. The illustration of the experimental setup is shown in Fig. 4, and the device specifications are given in Table III.

## A. Implementations

The experiment is carried out in an indoor environment. The height of the transmitters is 2.84 m. There are 12 circular luminaires mounted on the ceiling of the room to provide illumination and positioning information. As long as two luminaires are captured, whether they are complete or not, the user can be located. In the experiment, we manually mark the center and a mark point on each luminaire, and the mark points on one luminaire are shown in Fig. 4 (a). All the LEDs in a luminaire transmit the same information containing the luminaire's coordinate and ID.

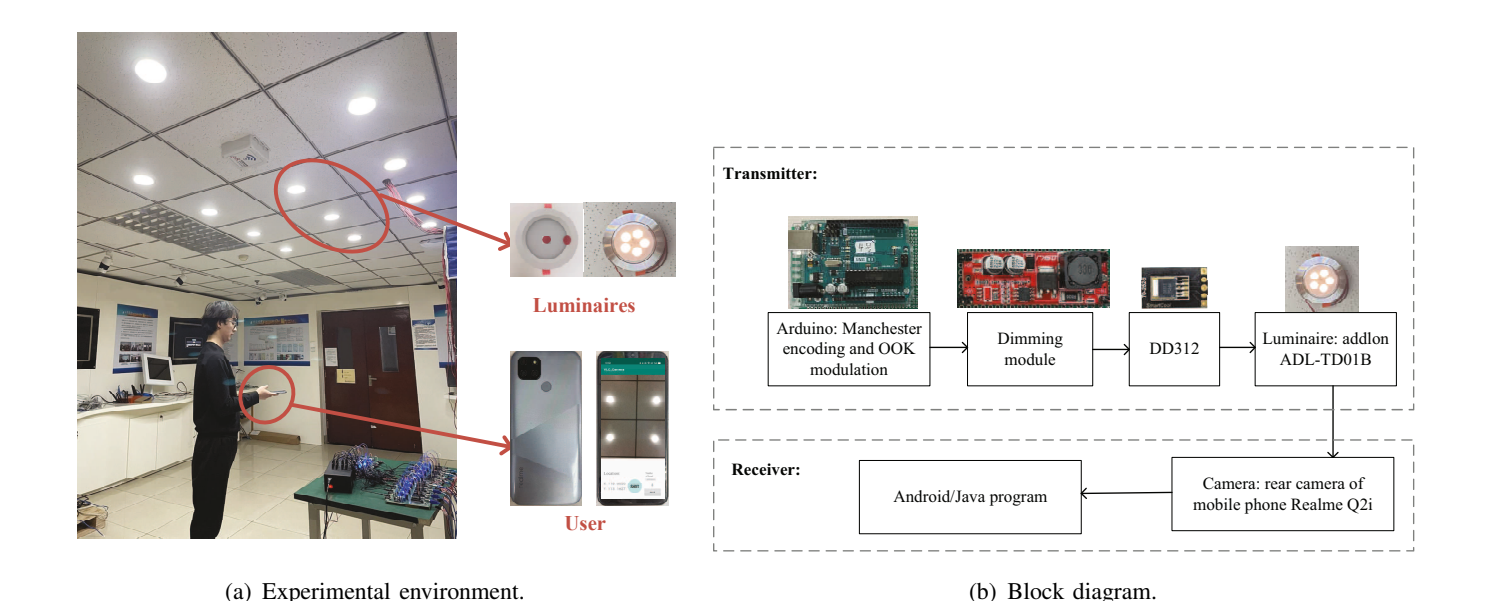


Fig. 4. Experimental setup.

TABLE III
DEVICE SPECIFICATIONS

]	Parameters	Model/Values
	Model	Addlon ADL-TD01B
Transmitter	Semi-angle, $\Phi_{1/2}$	67.5°
	Transmitter Power, $P_t$	5 W
	Radius	$3.5~\mathrm{cm}$
	Model	Rear camera of Realme Q2i
		f = 3.462 mm
Camera	Intrinsic parameters	$d_x = d_y = 1.12 \times 10^{-4} cm$
Camera		$(u_0, v_0) = (2080, 1560)$
	Resolution	$4160 \times 3120$
	Exposure time	1.25 ms & 6.67 ms

To successfully transmit the information, Arduino Studio is used to generate signals with Manchester encoding and on-off keying (OOK) modulation. Then, the dimming module is designed to control the transmitted power of the LED, after which, DD312, a constant current LED driver is used to drive the LED to emit light without flicking. In this way, the information of the transmitters are broadcasted to the air. To successfully receive the geometric information and the modulated VLC information that contain the IDs and world coordinates of the luminaires, a single camera is calibrated by a conventional method [39] to extract information from 2D images. We use rear complementary metal oxide semiconductor (CMOS) camera of Realme Q2i due to the exposure time requirement of the rolling shutter. We first leverage the rolling shutter effect of the CMOS image sensor to capture the fringe image of the luminaire, and we demodulate the fringes to receive the VLC information. Then, an image processing is implemented by an Android/Java program to receive the geometric information. Once an image is captured, the region of interest (ROI) is exploited for image processing to enhance the accuracy. After contour extraction and curve fitting, the elliptic curve equation and the pixel coordinates of the projections can be obtained from the processed images. Finally, the geometric feature information and the VLC information will be input into an Android/Java program, and the pose and location of the user can be output by implementing the proposed algorithm in the program.

# B. Image Processing

At the receiver side, both geometric feature information and VLC signals are supposed to be obtained. However, the fringe image that is easy to demodulate does not have enough clear outlines to fit the elliptic curve equation. For instance, Fig. 5 (a) is an original fringe image, which will turn into Fig. 5 (b) after filtering. It can be observed that the outline of Fig. 5 (b) is rather vague, which can lead to further detection errors as shown in Fig. 5 (c). Therefore, we propose a fused image processing scheme, and the

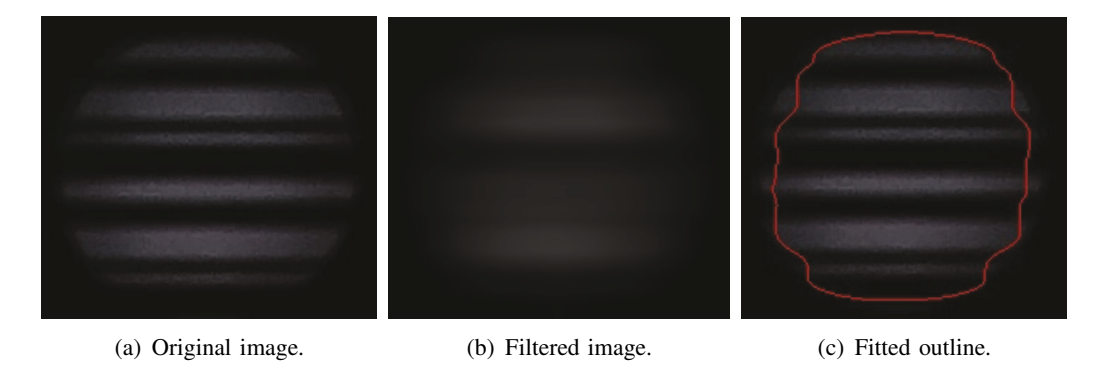


Fig. 5. Fringe images in image processing.

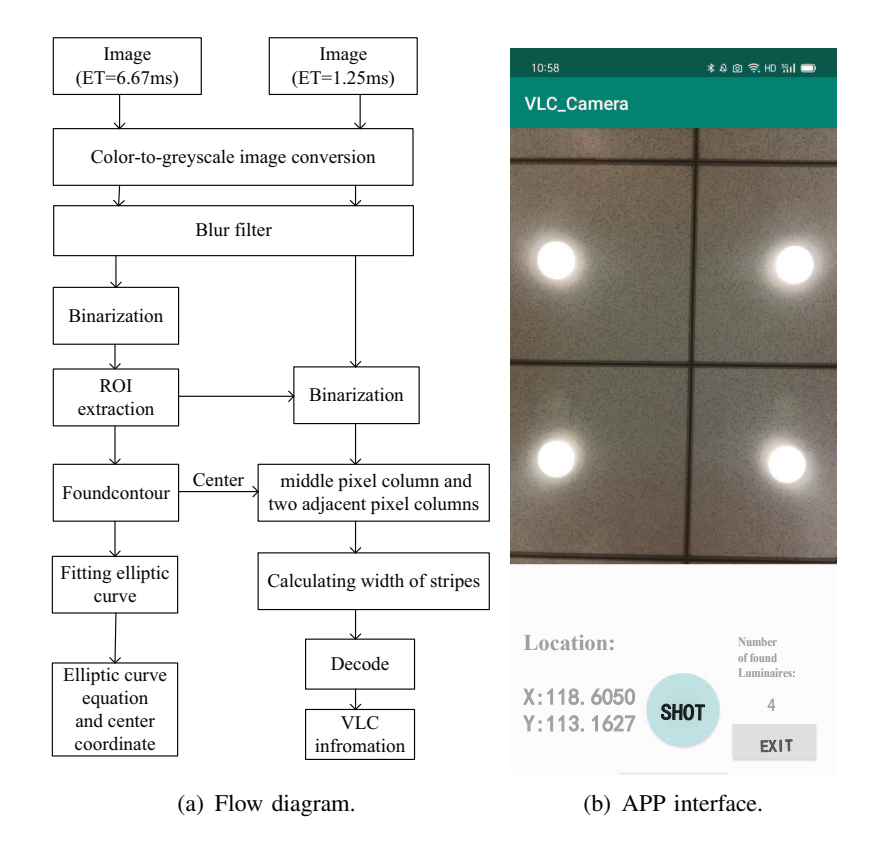
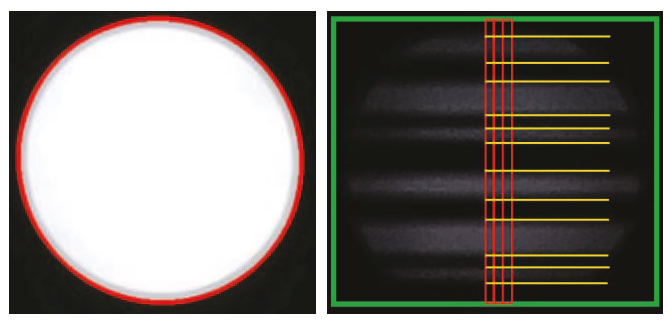


Fig. 6. Flow diagram of image processing and APP interface.

flow diagram is shown in Fig. 6 (a). In the proposed scheme, once a user needs to locate, the image sensor will take two photos under different exposure times (ET), and we develop an application as shown in Fig. 6 (b) for convenience. In this application, it can be automatically shoot under two ETs, and the interval between two ETs can be artificially controlled. When this interval is extremely short, the two captured images have approximately the same pose and location, and, thus, the pixel coordinates in two images are the same. Under a long ET, the luminaire is captured as a complete circle or an ellipse, while under a short ET, it is captured as a fringe image, as shown in Fig. 7 (a) and Fig. 7 (b), respectively.

Fig. 7 (a) and Fig. 7 (b) are used to obtain the geometric feature information and VLC signals as



(a) Image captured under a (b) Image captured under a short long exposure time (ET=6.67 exposure time (ET=1.25 ms). ms).

Fig. 7. Images in two-step image processing.

illustrated in Fig. 6 (a). First, Fig. 7 (a) and Fig. 7 (b) are converted from RGB images to greyscale images. For the images under the long ET, the filtered image is binarized to make the area of the bright region clear, so as to facilitate the ROI extraction. Since this image is considered to have the same pixels coordinates with the one under the short ET, the extracted ROIs can also be used in the image captured under the short ET. Then, Hough Transform [40] is used for object detection. The points on the ellipse contour, the projection point of the luminaire's center, and the projection point of the mark point are all extracted, and the extracted points on the contour are used to fit the elliptic curve equation with the least squares fitting. With this equation, the center of the ellipse can also be obtained according to (24) when the center or the mark point is not detected due to the occlusion. The occlusion can be detected by setting a threshold for a deviation distance between the extracted contour points and the fitted curve. For images under the short ET, a binarization process is performed in each ROI. The threshold of this binarization is higher than that under the long ET, since bright and dark fringes here have to be more distinguishable to reduce error in decoding. Then, according to the pixel coordinate of the center in the image, the middle pixel column and its two adjacent pixel columns are extracted, as shown in the regions of red boxes in Fig. 7 (b). The three pixel columns are selected here to reduce the calculation error. The widths of the bright and dark fringes in red boxes are further calculated. Then, the VLC signals are obtained by decoding the width values of the fringes.

### VI. SIMULATION AND EXPERIMENTAL RESULTS

In this section, we evaluate the performance of V-PCA and OA-V-PA via simulation and experimental results.

## A. Simulation Setup

We consider a rectangular room, in which four luminaires are deployed on the ceiling of the room. The system parameters are listed in Table IV. Unless otherwise specified, the radius of the LED luminaire is 15 cm. The image noise is defined as the deviation between the extracted feature points and the true contour, and this is modeled as a white Gaussian noise having an expectation of zero and a standard deviation of 2 pixels [22]. All statistical results are averaged over independent runs of 10,000 samples. For each simulation sample, the location and pose of the user are generated randomly in the room, and the tilted angle of the user is also generated randomly on the premise that at least two incomplete luminaires can be captured. To mitigate the impact of image noise, the pixel coordinate is obtained by processing 20 images for each location [22].

TABLE IV System parameters

Parameters	Values
LED semi-angle, $\Phi_{1/2}$	60°
Principal point of camera	$(u_0, v_0) = (320, 240)$
Physical sizes	$d_x = d_y = 1.25 \times 10^{-3}$
Room size	$8 \text{ m} \times 6 \text{ m} \times 3 \text{ m}$
Location of four LEDs (m)	(2,2,3), (6,2,3), (2,4,3), (6,4,3)

We evaluate the positioning performance in terms of location and pose accuracy. We define the location error as  $E_{\rm loc} = \| \boldsymbol{r}_{\rm true}^{\rm w} - \boldsymbol{r}_{\rm est}^{\rm w} \|$ , where  $\boldsymbol{r}_{\rm true}^{\rm w} = (x_{\rm true}^{\rm w}, y_{\rm true}^{\rm w}, z_{\rm true}^{\rm w})^{\rm T}$  and  $\boldsymbol{r}_{\rm est}^{\rm w} = (x_{\rm est}^{\rm w}, y_{\rm est}^{\rm w}, z_{\rm est}^{\rm w})^{\rm T}$  are true and estimated world coordinates of the user, respectively. In addition, with the true rotation  $\boldsymbol{R}_{\rm c,true}^{\rm w}$ , we quantify the relative error of the estimated pose,  $\boldsymbol{R}_{\rm c,est}^{\rm w}$ , by  $E_{\rm pos}\left(\%\right) = \|\boldsymbol{q}_{\rm true} - \boldsymbol{q}_{\rm est}\| / \|\boldsymbol{q}_{\rm est}\|$  [41], where  $\boldsymbol{q}_{\rm true}$  and  $\boldsymbol{q}_{\rm est}$  are the normalized quaternions of the true and the estimated rotation matrices, i.e.,  $\boldsymbol{R}_{\rm c,true}^{\rm w}$  and  $\boldsymbol{R}_{\rm c,est}^{\rm w}$ , respectively.

## B. Simulation Results

1) Effect of image noise and the luminaire's radius on positioning performance: In practice, since two captured luminaires can be complete or incomplete, both V-PCA and OA-V-PA algorithms may be used. Therefore, we evaluate the performance of V-PA that adaptively uses V-PCA and OA-V-PA according to the practical scenario, and we compare the positioning accuracy of V-PA with other existing algorithms. In terms of the number of required luminaires, we conduct PnP algorithm [42] as a baseline scheme. PnP algorithm is performed by analyzing more than four correspondences between 3D reference points and their 2D projections on the image, and it requires at least four LEDs for positioning. However, not all samples capture four luminaires simultaneously. Thus we select four LEDs evenly from two arcs captured

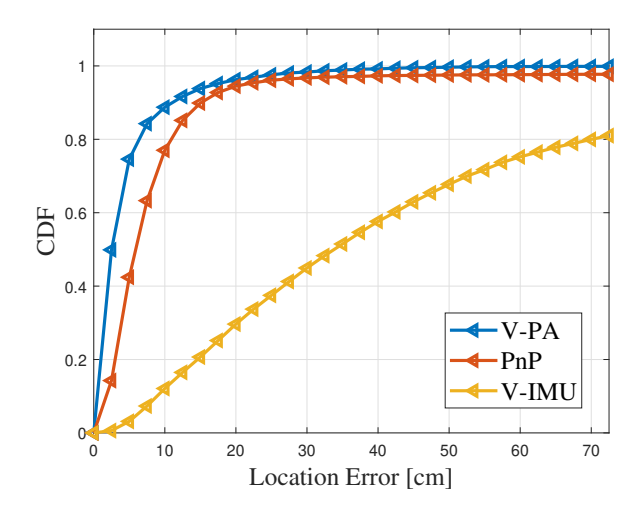


Fig. 8. CDF of the location error.

by the camera, such as the LEDs at the locations of M, N, P and Q on the luminaire in Fig. 2. To show the advantage of our algorithm that does not need extra device at the user, we conduct the IMU-based VLP (V-IMU) algorithm [27] as another baseline scheme. Note that IMU typically measures the pitch and roll angles with an error of  $1.5^{\circ}$ , and the azimuth angle with an error of  $15^{\circ}$  [29]. Therefore, for the V-IMU algorithm, we impose random measurement errors that satisfy the uniform distribution of  $[0, 1.5^{\circ}]$  on the pitch and roll angles, and random measurement errors that satisfy the uniform distribution of  $[0, 15^{\circ}]$  on the azimuth angle.

Fig. 8 compares the performance of our proposed algorithm with PnP and V-IMU algorithms in terms of the cumulative distribution function (CDF) of the location error. From this figure, we can observe that V-PA has the best performance among the three algorithms. As shown in Fig. 8, V-PA is able to achieve a 90th percentile accuracy of about 10 cm. In contrast, the PnP algorithm can achieve a 78th percentile accuracy of about 10 cm. Meanwhile, for the V-IMU algorithm, only a 16th percentile accuracy of about 10 cm is achieved. This is because the V-IMU algorithm requires the tilted angles to be small to achieve reliable approximation for the projection radius.

Fig. 9 shows the effect of image noise on V-PA in terms of the average  $E_{loc}$  and  $E_{pos}$ . The image noise is modeled as a white Gaussian noise with an expectation of zero and a standard deviation  $\sigma_n$  that ranges from 0 to 4 pixels. From Fig. 9 (a), we can observe that the average  $E_{loc}$  is 0 cm when  $\sigma_n$  is 0 for V-PA and PnP. That indicates that the location errors of them are totally caused by the image noise. The average  $E_{loc}$  of V-IMU increases from 31 cm to 61 cm as the image noise increases from 0 to 4 pixels, while that of PnP increases from 0 cm to 37 cm. Besides, as the image noise increases, the average  $E_{loc}$  of V-PA varies in a relative small range, from 0 cm to 10 cm, which indicates that V-PA is more robust to image

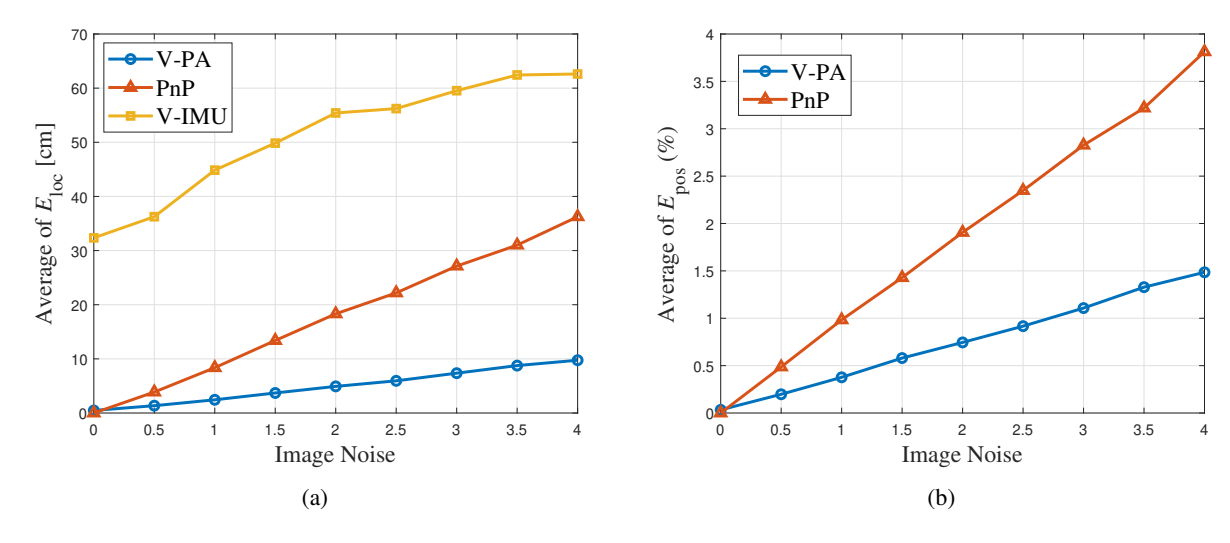


Fig. 9. The mean of  $E_{\rm loc}$  and  $E_{\rm pos}$  versus the image noise.

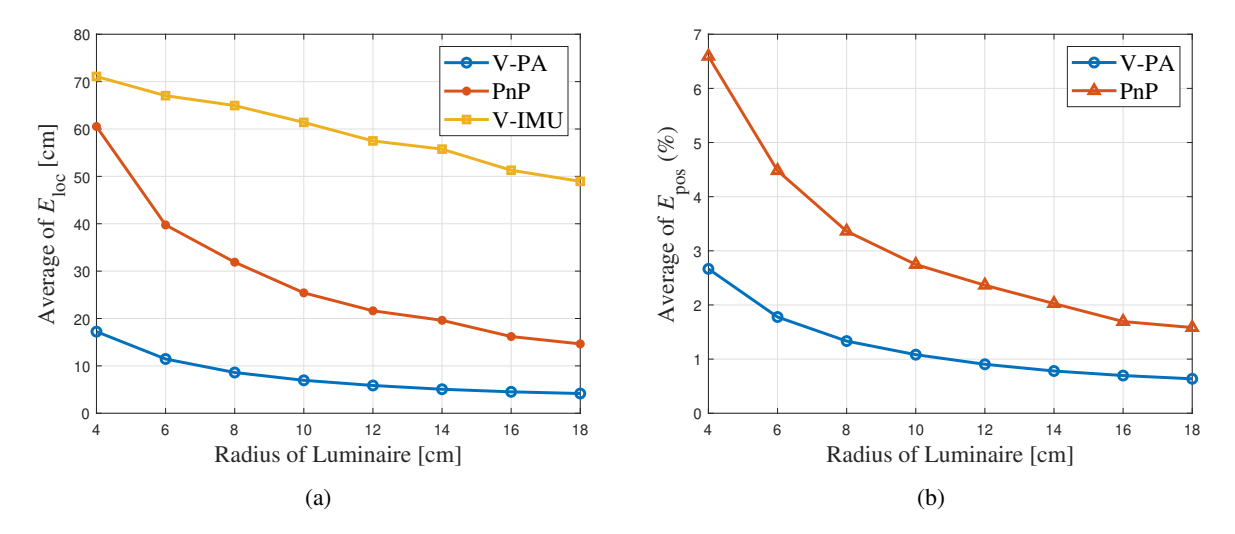


Fig. 10. The mean of  $E_{\rm loc}$  and  $E_{\rm pos}$  versus the radius of the luminaire.

noise. In addition, Fig. 9 (b) further illustrates the average  $E_{pos}$  versus the image noise. The average  $E_{pos}$  of V-PA increases from 0% to 1.5% as radius increases, while that of PnP increases from 0% to 3.8%. These results also verify that, compared with the PnP algorithm, V-PA is more robust to image noise.

Fig. 10 evaluates the effect of the radius of the luminaire on positioning accuracy. This performance is captured by the average  $E_{loc}$  and the average  $E_{pos}$  with the radius varying from 4 cm to 18 cm. As shown in Fig. 10 (a), the accuracy of location estimation improves as the radius of luminaire increases. V-PA has the best performance among the three algorithms. For V-PA, the average  $E_{loc}$  remains below 18 cm for all radii. For PnP, the average  $E_{loc}$  decreases from 61 cm to 15 cm as the radius of the luminaire increases. Meanwhile, for V-IMU, the average  $E_{loc}$  decreases from 70 cm to 49 cm. We can observe that, when the radius is below 8 cm, the average  $E_{loc}$  of both V-PA and PnP decreases fast as radius increases.

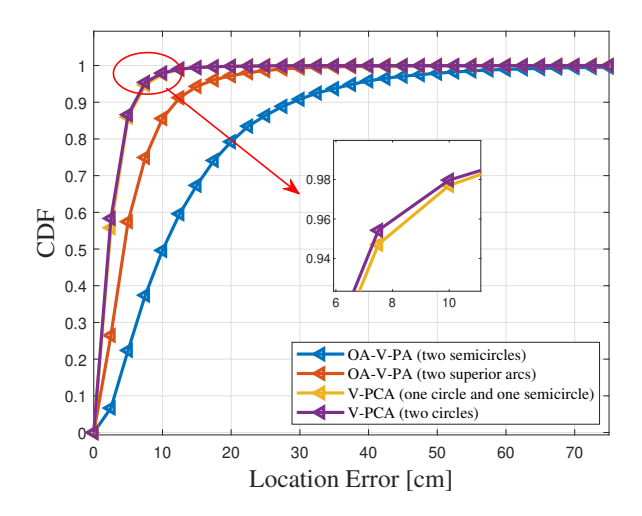
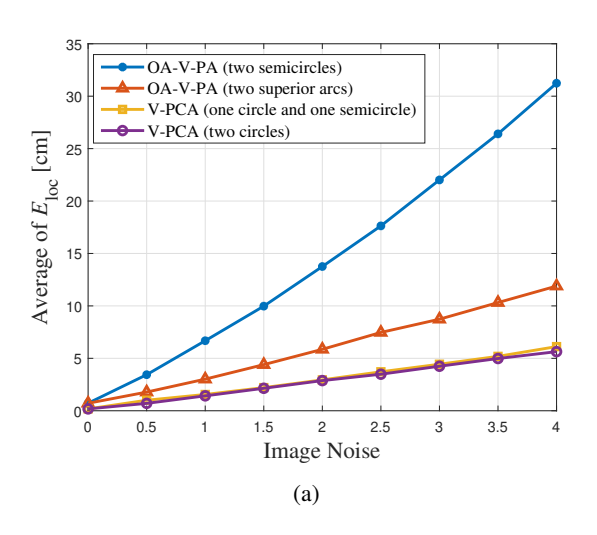


Fig. 11. Cumulative Distribution Function (CDF) of the location error.

This is due to the fact that, when the captured geometric features have small size, the positioning accuracy is affected by the image noise more seriously. Fig. 10 (b) compares the average  $E_{\rm pos}$  of V-PA and PnP. Here, we observe V-PA is more accurate than PnP. The average  $E_{\rm pos}$  of V-PA decreases from 2.8% to 0.7% as the radius increases, while that of PnP decreases from 6.6% to 1.7%. This also indicates that the pose accuracy of the PnP algorithm is affected more by the small size of luminaire than that of the V-PA algorithm.

2) Effect of the arc length of the captured luminaires on positioning performance: We then also compare the positioning performance of V-PCA and OA-V-PA algorithms, in which, we evaluate how the length of the contours that extracted from the captured luminaires affect the positioning performance. For comparison, we conduct four schemes: i) OA-V-PA with two semicircles extracted, ii) OA-V-PA with two superior arcs extracted, iii) V-PCA with a circle and a semicircle extracted, and iv) V-PCA with two circles extracted. For each scheme, we use the same samples for fairness, and each sample captures two complete luminaires. This means that V-PCA and OA-V-PA capture the same information at the same position with the same tilted angle, while they use different arc information for positioning.

Fig. 11 compares the performance of V-PCA and OA-V-PA in terms of the CDF of the location error. We observe that V-PCA performs better than OA-V-PA. The performance of the two V-PCA schemes are close, and the performance of V-PCA with two circles is slightly better than that of V-PCA with a circle and a semicircle. V-PCA schemes are able to achieve a 97th percentile accuracy of about 10 cm, which is slightly better than the performance of V-PA in Fig. 8. This is because OA-V-PA is also adaptively selected together with V-PCA in Fig. 8. As shown in Fig. 8, OA-V-PA with two semicircles can achieve an 86th percentile accuracy of about 10 cm, while OV-V-PA with two superior arcs can only achieve a



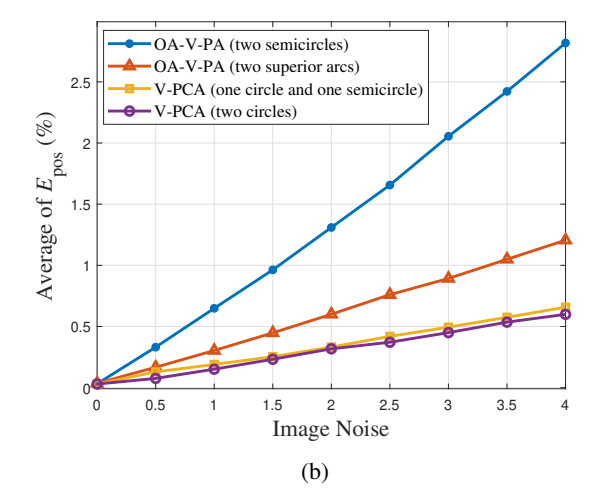
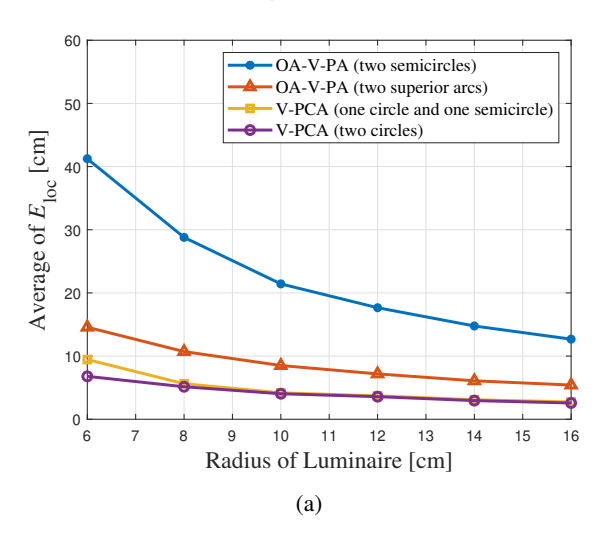


Fig. 12. The mean of  $E_{\rm loc}$  and  $E_{\rm pos}$  versus the image noise.



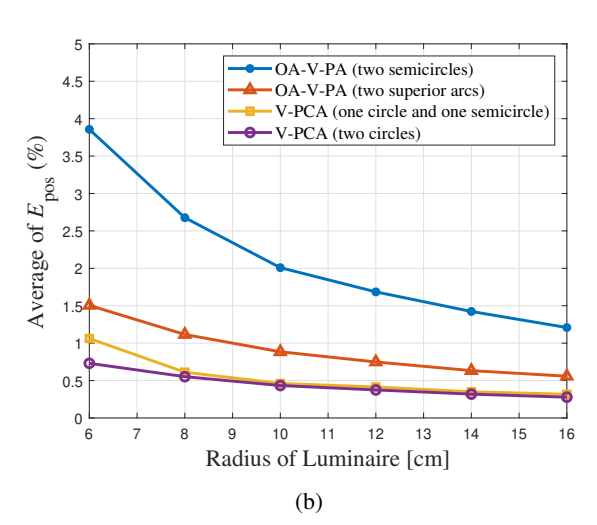


Fig. 13. The mean of  $E_{\rm loc}$  and  $E_{\rm pos}$  versus the radius of the luminaire.

50th percentile accuracy of about 10 cm. Therefore, the location accuracy improves as the available arc length of captured luminaire increases.

Fig. 12 shows the effect of the arc length of the extracted contour on positioning accuracy as image noise increases. The image noise is modeled with a standard deviation  $\sigma_n$  that ranges from 0 to 4 pixels. From Fig. 12(a), we can observe that the average  $E_{loc}$  is 0 cm when  $\sigma_n$  is zero for V-PCA, while it is about 0.7 cm for OA-V-PA. This is because, in OA-V-PA, the projection of the luminaires center is an approximative value, which leads to slight deviations. Moreover, the average  $E_{loc}$  of OA-V-PA with two semicircles increases from 0.7 cm to 31.2 cm as the image noise increases from 0 to 4 pixels, while that of OA-V-PA with two superior arcs increases from 0.7 cm to 11.8 cm. For V-PCA with a circle and a semicircle, the average  $E_{loc}$  increases from 0 cm to 5.6 cm, while it increases from 0 cm to 6.1 cm for

V-PCA with two circles. Fig. 12 (b) further illustrates the average  $E_{pos}$  versus the image noise. Here, we can see that the average  $E_{pos}$  of all schemes increase as the image noise increases. Both Fig. 12 (a) and Fig. 12 (b) indicate that the robustness to image noise increases when the arc length of captured luminaire increases. In the situation in which a complete circle is captured, this change is not obvious whether the other captured luminaire is complete or incomplete. This is due to the fact that the other captured luminaire is only used to eliminate the duality of the normal vector but not estimate the location of the user.

Fig. 13 evaluates the effect of the arc length of the extracted contour on positioning accuracy as the radius of the luminaire increases. The radius varies from 6 cm to 16 cm. As shown in Fig. 13, V-PCA with two circles has the best performance in terms of the average  $E_{loc}$  and the average  $E_{pos}$ . In Fig. 13 (a), the average  $E_{loc}$  of OA-V-PA with two semicircles decreases from 41.2 cm to 12.7cm, while the average  $E_{loc}$  of OA-V-PA with two superior arcs decreases from 14.6 cm to 5.4 cm. We can also observe that the averages of  $E_{loc}$  of two V-PCA schemes are both below 10 cm. Fig. 13 (b) compares the average  $E_{pos}$  of OV-V-PA and V-PCA versus the radius of luminaire. We can observe that V-PCA performs better than OA-V-PA. This also verifies that the positioning performance increases as the arc length of the captured luminaire increases. Although the accuracy of OA-V-PA is slightly lower than V-PCA, it improves as the arc length of the captured luminaire increases.

## C. Experimental Results

This subsection evaluates the accuracy of V-PA via practical experiments. To verify the performance of V-PA, we estimate the locations of 16 points uniformly distributed in a 180 cm × 210 cm test area. At each reference point, the smartphone is fixed on a tripod in order to ensure the accuracy of the user's coordinates. The coordinates in cm of the reference points are (45, 30), (45, 90), (45, 150), (45, 210), (90, 30), (90,90), (90, 150), (90, 210), (135, 30), (135, 90), (135, 150), (135, 210), (180, 30), (180, 90), (180, 150) and (180, 210), which also represent the location of the center of the smartphone. For each test point, we locate the user for 10 times. In the experiments, we compare the performance of our algorithm with V-IMU. We also evaluate the effect of heights and tilted angles of the user on the 3D positioning accuracy and the robustness.

Fig. 14 compares the experimental performance of our proposed algorithm with V-IMU in terms of the CDF of the location error. The tilted angle is 0° and the height of the user is 120 cm. It can be observed that our positioning algorithm outperforms V-IMU. In particular, V-PA is able to achieve less than 10 cm positioning errors for 100th percentile test points, while V-IMU can achieve a 50th percentile accuracy of about 10 cm.

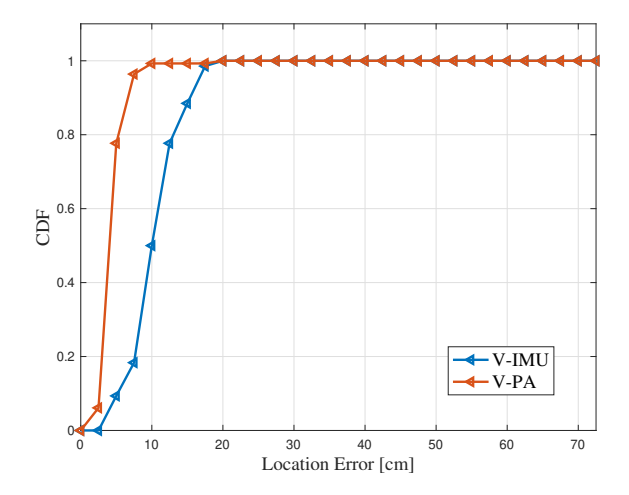


Fig. 14. CDF of the experimental location error.

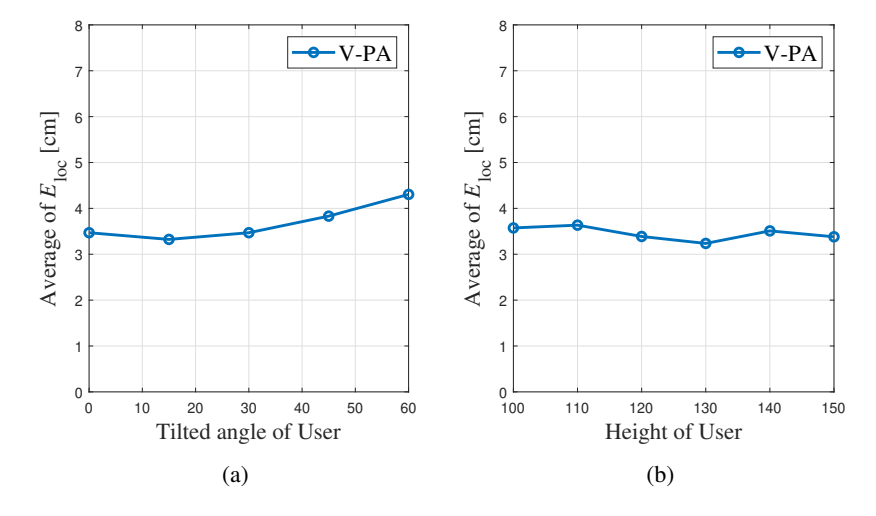


Fig. 15. The mean of experimental  $E_{\rm loc}$  versus the tilted angle and height of the user.

Fig. 15 (a) shows the average location error versus the tilted angle of the user. Due to the challenge in measuring the three rotation angles of orientation, we only tilt the smartphone around its bottom edge with different angles. Hence, we only need to measure a tilted angle to evaluate the effect of the tilted angles on positioning performance. From Fig. 15 (a), it can be observed that as the tilted angle increases, the mean of the location error also increases. This is because that when the tilted angle increases, the eccentricity of the projection ellipse also increases. Hence, the approximation error of the projection of the luminaire's center increases and leads to positioning error. However, the mean of the location error increases in a relative small range, i.e. from 3 cm to 5 cm. Therefore, the tilted angle of the user has little effect on the positioning performance. Fig. 15 (b) shows the average location error versus the height of the user. The tilted angle of the user is 0°. It can be observed that as the height of the user increases, the

mean of the location error slightly varies between 3 and 4 cm. This verifies that positioning performance is robust to the variations of the height of the users.

Fig. 16 shows the positioning performance of the proposed scheme as tilted angle and height of the user change. It can be observed that the positioning accuracy varies slightly when the tilted angle and height change, which is aligned with Figs. 15 (a) and 15 (b), thus further verifying the robustness of V-PA.

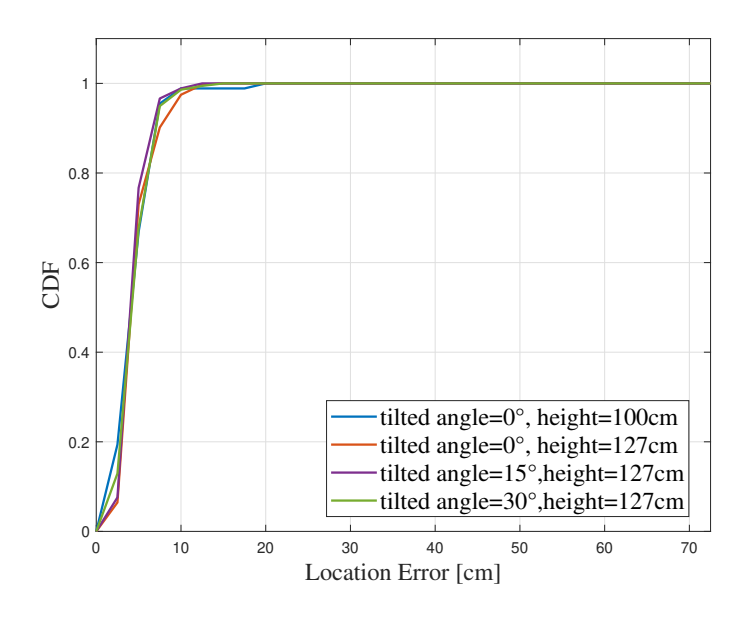


Fig. 16. CDF of the positioning accuracies under different settings.

## VII. CONCLUSION

In this paper, we have proposed a practical V-PA approach for indoor positioning, which can achieve pose and location estimation of the user using circular luminaires. The proposed approach does not need IMU and has no tilted angle limitations at the user. In particular, we have first developed an algorithm called V-PCA, in which, the geometric features extracted from a complete circular luminaire and an incomplete one have been developed for the pose and location estimation. Furthermore, we have proposed the OA-V-PA algorithm to enhance the practicality and robustness when part VLC links are blocked. We have also established a prototype, in which a fused image processing scheme was proposed to simultaneously obtain VLC signals and geometric information. Simulation results show that V-PA can achieve a 90th percentile positioning accuracy of around 10 cm. The experimental results also show that the average location error is less than 5 cm whether the user is tilted or vertically upward. Therefore, V-PA is promising for indoor positioning, which is practical and suitable for common indoor scenarios.

### REFERENCES

- [1] Z. Zhu, Y. Yang, C. Guo, C. Feng, and B. Jia, "Visible light communication assisted perspective circle and arc algorithm for indoor positioning," in *Proc. IEEE International Conference on Communications (ICC)*, Soul, South Korea, 2022, pp. 3832–3837.
- [2] W. Saad, M. Bennis, and M. Chen, "A vision of 6G wireless systems: Applications, trends, technologies, and open research problems," *IEEE Network*, vol. 34, no. 3, pp. 134–142, May 2020.
- [3] Z. Jiao, B. Zhang, M. Liu, and C. Li, "Visible light communication based indoor positioning techniques," *IEEE Netw.*, vol. 31, no. 5, July 2017.
- [4] L. E. M. Matheus, A. B. Vieira, L. F. M. Vieira, M. A. M. Vieira, and O. Gnawali, "Visible light communication: Concepts, applications and challenges," *IEEE Commun. Surveys Tuts.*, vol. 21, no. 4, pp. 3204–3237, Fourthquarter 2019.
- [5] Y. Yang, Z. Zeng, J. Cheng, C. Guo, and C. Feng, "A relay-assisted OFDM system for VLC uplink transmission," *IEEE Trans. Commun.*, vol. 67, no. 9, pp. 6268–6281, Sep. 2019.
- [6] T.-H. Do and M. Yoo, "An in-depth survey of visible light communication based positioning systems," Sensors, vol. 16, no. 5, p. 678, May. 2016.
- [7] C. Sertthin, T. Ohtsuki, and M. Nakagawa, "6-axis sensor assisted low complexity high accuracy-visible light communication based indoor positioning system," *IEICE Trans. Commun.*, vol. 93, no. 11, pp. 2879–2891, Nov. 2010.
- [8] F. Alam, M. T. Chew, T. Wenge, and G. S. Gupta, "An accurate visible light positioning system using regenerated fingerprint database based on calibrated propagation model," *IEEE Trans. Instrum. Meas.*, vol. 68, no. 8, pp. 2714–2723, Aug. 2018.
- [9] A. H. A. Bakar, T. Glass, H. Y. Tee, F. Alam, and M. Legg, "Accurate visible light positioning using multiple-photodiode receiver and machine learning," *IEEE Trans. Instrum. Meas.*, vol. 70, pp. 1–12, Sep. 2020.
- [10] F. Alam, M. T. Chew, T. Wenge, and G. S. Gupta, "An accurate visible light positioning system using regenerated fingerprint database based on calibrated propagation model," *IEEE Trans. Instrum. Meas.*, vol. 68, no. 8, pp. 2714–2723, Aug. 2018.
- [11] L. Bai, Y. Yang, C. Guo, C. Feng, and X. Xu, "Camera assisted received signal strength ratio algorithm for indoor visible light positioning," *IEEE Commun. Lett.*, vol. 23, no. 11, pp. 2022–2025, Nov. 2019.
- [12] S. Li, S. Shen, and H. Steendam, "A positioning algorithm for VLP in the presence of orientation uncertainty," *Signal Process.*, vol. 160, pp. 13–20, July 2019.
- [13] B. Zhou, A. Liu, and V. Lau, "Performance limits of visible light-based user position and orientation estimation using received signal strength under nlos propagation," *IEEE Trans. Wireless Commun.*, vol. 18, no. 11, pp. 5227–5241, Nov. 2019.
- [14] T. Q. Wang, Y. A. Sekercioglu, A. Neild, and J. Armstrong, "Position accuracy of time-of-arrival based ranging using visible light with application in indoor localization systems," *J. Lightw. Technol.*, vol. 31, no. 20, pp. 3302–3308, Oct. 2013.
- [15] B. Zhu, J. Cheng, Y. Wang, J. Yan, and J. Wang, "Three-dimensional VLC positioning based on angle difference of arrival with arbitrary tilting angle of receiver," *IEEE J. Sel. Areas Commun.*, vol. 36, no. 1, pp. 8–22, Jan. 2017.
- [16] B. Soner and S. Coleri, "Visible light communication based vehicle localization for collision avoidance and platooning," *IEEE Trans. Veh. Technol.*, vol. 70, no. 3, pp. 2167–2180, Mar. 2021.
- [17] K. Aalimahmoodi, A. Gholami, and Z. Ghassemlooy, "An image sensor based indoor VLP system," in *IEEE International Symposium on Telecommunications (IST)*, Tehran, Iran, 2018, pp. 371–374.
- [18] J. Fang, Z. Yang, S. Long, Z. Wu, X. Zhao, F. Liang, Z. L. Jiang, and Z. Chen, "High-speed indoor navigation system based on visible light and mobile phone," *IEEE Photon. J.*, vol. 9, no. 2, pp. 1–11, Apr. 2017.
- [19] Y. Zhuang, L. Hua, L. Qi, J. Yang, P. Cao, Y. Cao, Y. Wu, J. Thompson, and H. Haas, "A survey of positioning systems using visible LED lights," *IEEE Commun. Surveys Tuts.*, vol. 20, no. 3, pp. 1963–1988, Thirdquarter 2018.
- [20] J. Luo, L. Fan, and H. Li, "Indoor positioning systems based on visible light communication: State of the art," *IEEE Commun. Surveys Tuts.*, vol. 19, no. 4, pp. 2871–2893, Fourthquarter 2017.

- [21] W. Guan, X. Zhang, Y. Wu, Z. Xie, J. Li, and J. Zheng, "High precision indoor visible light positioning algorithm based on double LEDs using CMOS image sensor," *Appl. Sci.*, vol. 9, no. 6, p. 1238, Mar. 2019.
- [22] L. Bai, Y. Yang, M. Chen, C. Feng, C. Guo, W. Saad, and S. Cui, "Computer vision-based localization with visible light communications," *IEEE Trans. Wireless Commun.*, vol. 21, no. 3, pp. 2051–2065, Mar. 2021.
- [23] L. Bai, Y. Yang, C. Feng, and C. Guo, "Received signal strength assisted perspective-three-point algorithm for indoor visible light positioning," *Opt. Exp.*, vol. 28, no. 19, pp. 28 045–28 059, Nov. 2020.
- [24] S. Pergoloni, Z. Mohamadi, A. M. Vegni, Z. Ghassemlooy, and M. Biagi, "Metameric indoor localization schemes using visible lights," *J. Lightw. Technol.*, vol. 35, no. 14, pp. 2933–2942, July 2017.
- [25] Y. Yang, C. Li, R. Bao, C. Guo, C. Feng, and J. Cheng, "Multi-angle camera assisted received signal strength algorithm for visible light positioning," *J. Lightw. Technol.*, Dec. 2021.
- [26] R. Zhang, W.-D. Zhong, Q. Kemao, and S. Zhang, "A single LED positioning system based on circle projection," *IEEE Photon. J.*, vol. 9, no. 4, pp. 1–9, Aug. 2017.
- [27] H. Cheng, C. Xiao, Y. Ji, J. Ni, and T. Wang, "A single LED visible light positioning system based on geometric features and CMOS camera," *IEEE Photon. Technol. Lett.*, vol. 32, no. 17, pp. 1097–1100, Sep. 2020.
- [28] Y. Wang, B. Hussain, and C. Patrick Yue, "Arbitrarily tilted receiver camera correction and partially blocked LED image compensation for indoor visible light positioning," *IEEE Sensors J.*, vol. 22, no. 6, pp. 4800–4807, Mar. 2021.
- [29] J. Hao, J. Chen, and R. Wang, "Visible light positioning using a single LED luminaire," *IEEE Photon. J.*, vol. 11, no. 5, pp. 1–13, Oct. 2019.
- [30] V. Popescu, P. Rosen, L. Arns, X. Tricoche, C. Wyman, and C. M. Hoffmann, "The general pinhole camera: Effective and efficient nonuniform sampling for visualization," *IEEE Trans. Vis. Comput. Graphics*, vol. 16, no. 5, pp. 777–790, Sep. 2010.
- [31] P. Sturm, "Pinhole camera model. computer vision: A reference guide," 2014.
- [32] A. Zisserman, "Geometric framework for vision i: Single view and two-view geometry," *Lecture Notes, Robotics Research Group, University of Oxford*, 1997.
- [33] A. Fitzgibbon, M. Pilu, and R. B. Fisher, "Direct least square fitting of ellipses," *IEEE Trans. Pattern Anal. Mach. Intell*, vol. 21, no. 5, pp. 476–480, May 1999.
- [34] L. Olson and M. Yu, "Least squares data fitting," https://courses.grainger.illinois.edu/cs357/fa2022/notes/ref-17-least-squares.html.
- [35] R. Safaee-Rad, I. Tchoukanov, K. C. Smith, and B. Benhabib, "Three-dimensional location estimation of circular features for machine vision," *IEEE Trans. Robot. Autom.*, vol. 8, no. 5, pp. 624–640, Oct. 1992.
- [36] E. W. Weisstein, "Quadratic surface. from mathworld—a wolfram web resource," 1999.
- [37] Y. Li, Z. Ghassemlooy, X. Tang, B. Lin, and Y. Zhang, "A VLC smartphone camera based indoor positioning system," *IEEE Photon. Technol. Lett.*, vol. 30, no. 13, pp. 1171–1174, July 2018.
- [38] Y. Yang, C. Wang, C. Feng, C. Guo, J. Cheng, and Z. Zeng, "A generalized dimming control scheme for visible light communications," *IEEE Trans. Commun.*, vol. 69, no. 3, pp. 1845–1857, Mar. 2021.
- [39] L. Zhou, Y. Yang, M. Abello, and M. Kaess, "A robust and efficient algorithm for the PnL problem using algebraic distance to approximate the reprojection distance," in *Proc. the AAAI Conference on Artificial Intelligence*, vol. 33, no. 01, 2019, pp. 9307–9315.
- [40] D. H. Ballard, "Generalizing the hough transform to detect arbitrary shapes," Pattern recognit., vol. 13, no. 2, pp. 111–122, Sep. 1980.
- [41] V. Lepetit, F. Moreno-Noguer, and P. Fua, "Epnp: An accurate o(n) solution to the PnP problem," *Int. J. Comput. Vis.*, vol. 81, no. 2, p. 155, July 2009.
- [42] X. Lu, "A review of solutions for perspective-n-point problem in camera pose estimation," *J. Phys., Conf. Ser.*, vol. 1087, no. 5, p. 052009, Sep. 2018.